Review Article

Manal M. Alsalama*, Hicham Hamoudi, Ahmed Abdala, Zafar K. Ghouri, and Khaled M. Youssef

Enhancement of Thermoelectric Properties of Layered Chalcogenide Materials

https://doi.org/10.1515/rams-2020-0023
Received Dec 24, 2019; accepted Apr 27, 2020

Abstract: Thermoelectric materials have long been proven to be effective in converting heat energy into electricity and vice versa. Since semiconductors have been used in the thermoelectric field, much work has been done to improve their efficiency. The interrelation between their thermoelectric physical parameters (Seebeck coefficient, electrical conductivity, and thermal conductivity) required special tailoring in order to get the maximum improvement in their performance. Various approaches have been reported in the research for developing thermoelectric performance, including doping and alloying, nanostructuring, and nanocompositing. Among different types of thermoelectric materials, layered chalcogenide materials are unique materials with distinctive properties. They have low self-thermal conductivity, and their layered structure allows them to be modified easily to improve their thermoelectric performance. In this review, basic knowledge of thermoelectric concepts and challenges for enhancing the figure of merit is provided. It discusses briefly different groups of layered chalcogenide thermoelectric materials with their structure and thermoelectric properties. It also reports different approaches in the literature for improving their performance and the recent progress done in this field. It highlights graphene as a promising nano additive to layered chalcogenide materials' matrix and shows its effect on enhancing their figure of merit.

Keywords: Thermoelectric materials, layered chalcogenides, nanocomposites, nanostructuring, figure of merit

1 Introduction

The demand for clean and sustainable energy sources is a growing global concern as the cost of energy is rapidly increasing; fossil fuel sources have been shown to affect the environment. Considering that a large amount of our utilized energy is in the form of heat and that a large amount of other forms of utilized energy is wasted as heat, the search for a suitable technology to recover this wasted heat and limit its harmful effects is essential. Among several technologies used to meet these demands, thermoelectric energy is considered to be of the most interest due to its unique capabilities. Thermoelectric generators can convert wasted heat into electrical energy. Conversely, they can transform electrical energy into thermal energy for refrigeration applications. The thermoelectric performance of thermoelectric materials is evaluated by the dimensionless figure of merit, ZT.

$$ZT = \frac{S^2 \sigma}{k_{tot}} \quad (1)$$

where S is the Seebeck coefficient, σ is electrical conductivity, k_{tot} is total thermal conductivity, and $S^2\sigma$ is the power factor.

Thermoelectric materials have several advantages; these materials are simple, solid-state devices, involve toxic-free operation, have no moving parts or chemical reactions, and demonstrate the potential for scalability. Besides, thermoelectric materials produce negligible amounts of greenhouse gas emissions. However, commercial applications of thermoelectric materials are limited because of the low efficiency relative to the cost, which is inadequate to compete with conventional power generation [1]. As a result, extensive work has been done to achieve high efficiency and widespread applications of thermoelectric materials.

The first generation of bulk thermoelectric materials has low efficiency. The interdependence of thermoelectric properties led to concerted efforts to develop strategies in the past decade to enhance thermoelectric efficiency, including improving the Seebeck coefficient and electrical conductivity as well as reducing thermal conductivity. Several strategies, including nanostructuring and nanocom-

***Corresponding Author: Manal M. Alsalama:** Department of Sustainable Development, Hamad Bin Khalifa University, Doha 5825, Qatar; Email: mmalsalama@mail.hbku.edu.qa; Tel.: +974 50319955
Hicham Hamoudi: Qatar Environment and Energy Research Institute, Doha 34110, Qatar
Ahmed Abdala, Zafar K. Ghouri: Department of Chemical Engineering, Texas A&M University, Doha 23874, Qatar
Khaled M. Youssef: Department of Materials Science and Technology, Qatar University, Doha 2713, Qatar

positing, have been developed and have led to remarkable progress in enhancing thermoelectric performance and the efficiency of thermoelectric materials [2].

Various materials have been used for thermoelectricity over a wide range of temperatures, including polymeric and inorganic materials. However, inorganic semiconducting materials were found to be the most efficient for thermoelectric applications [3, 4]. Among inorganic materials, layered chalcogenides have attracted attention as they demonstrate high *ZT* values with high electrical properties and low thermal conductivity [2]. Layered materials exhibit layered structure with strong covalent bonds within the layer and weak van der Waals forces between the layers. The layered structure provides a way to separate the movement of charge carriers and phonons; charge carriers could effectively move within the layers while the phonons may scatter significantly between the layers due to the presence of weak van der Waals forces. Several strategies can be used to improve thermoelectric properties, such as doping, alloying, nanostructuring, and nanocompositing [5, 6].

The *ZT* value has been improved by creating different nanostructured materials with different shapes and forms such as nano-bulk, quantum dots, nanowires, and nanofilms. The high density of the grain boundaries presented in those materials results in exceptional thermoelectric properties. Grain boundaries play an important role in reducing lattice thermal conductivity by phonon scattering as well as in modifying electrical properties by energy filtering low carriers. Compared with conventional-sized materials, engineering of nanostructuring boosted the efficiency of thermoelectric materials to a new level for several thermoelectric systems. The breakthrough in nanotechnology demonstrates the advantages to improve thermoelectric performance that led to a burst in the field of thermoelectric nanomaterials [7].

Nanocomposites, which include a combination of multiple materials of which at least one has a nanometer dimension, have gained considerable attention as well. Layered chalcogenide thermoelectric materials have been mixed with several additive materials. It has been found that incorporating nano additive as a second phase of the thermoelectric material matrix is a simple top-down approach that allows optimization of thermoelectric properties to improve electrical properties and reduce thermal conductivity. However, selecting the type of additive is an important step to achieve the best possible improvement in electrical properties and the best possible reduction in electrical conductivity. These requirements open the door to the search for nano additives with excellent electrical properties in order to improve power factors as well as to contribute to a reduction in thermal conductivity due to their nanosize.

Graphene is a two-dimensional sheet that is one atom thick with superior electrical and thermal properties. It has attracted the attention of researchers since its discovery in 2004 [8]. The availability of bulk quantities of high-quality graphene [9] makes it a suitable material that can be utilized as an additive for preparing different functional thermoelectric composites with different matrix materials [10, 11]. A small amount of graphene embedded into the thermoelectric matrix can play an essential role in enhancing the efficiency of the thermoelectric composites [12]. However, among layered chalcogenide materials, graphene has been used recently as an additive for bismuth telluride.

The aim of this review is to conduct a comprehensive study of layered chalcogenide materials and the recent work and progress made for improving their figure of merit. First, it discusses thermoelectric properties and different types of thermoelectric materials. Then it discusses in detail, layered chalcogenide thermoelectric materials, by giving a basic knowledge of their structure and thermoelectric properties. It summarizes the effect of different mechanisms used in the literature to improve their *ZT*, including doping and alloying, nanostructuring, and nanocompositing. It sheds light on graphene as a distinctive material that is used in the field of thermoelectricity to improve thermoelectric properties. Finally, it overviews graphene bismuth telluride composites and how their thermoelectric behavior is affected by the addition of graphene. The limited work on graphene composites showing significant improvement has inspired further work for enhancing other layered chalcogenide materials and thermoelectric materials.

2 Thermoelectric Materials, Basic Theory and Categories

Thermoelectric materials were discovered in the 18th century, and since then, many developments have been achieved. The history of thermoelectric materials is characterized by the progress of the figure of merit (*ZT*) [1, 13, 14], which is a thermoelectric quantity related to the conversion efficiency of thermoelectric materials. Three main properties are contributed to the value of *ZT*, Seebeck coefficient, electrical conductivity and thermal conductivity. Seebeck coefficient is an electrical property defined as the amount of voltage generated per unit of temperature differ-

ence, in units of V/K. Figure 1 illustrates the concept of the Seebeck effect [3].

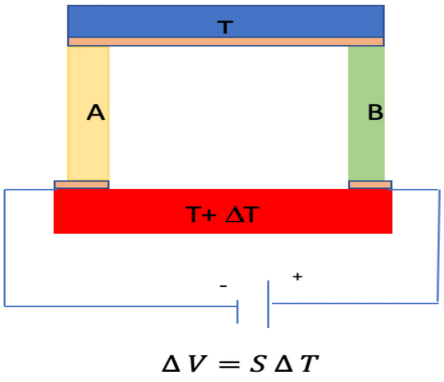

Figure 1: Simple diagram illustrating the Seebeck effect. Material A and material B are subjected to temperature difference ΔT, which induced a voltage difference ΔV.

Electrical conductivity is the ability of the charge carriers to travel through the material under an applied electric field and is given by:

$$\sigma = ne\mu \tag{2}$$

where n is the concentration of charge carriers, e is the magnitude of the electron charge, and μ is the charge carrier mobility. Thermal conductivity is the energy induced from applied temperature and transported through the material by both phonons and charge carriers. Thermal conductivity is the sum of the heat transported by charge carriers (k_e) and traveling of phonons through the lattice (k_l). If one type of charge carrier is predominant, then $k_{tot} = k_e + k_l$. Good thermoelectric materials should possess as high ZT as possible; therefore, it is reasonable to expect that materials with high electrical conductivity, a high Seebeck coefficient, and low thermal conductivity are required for thermoelectric applications. However, materials that possess all these properties simultaneously are not available in nature. Metals have high electrical conductivity but low Seebeck coefficient and high thermal conductivity. Insulators exhibit low thermal conductivity and poor electrical conductivity. Hence, optimizing all thermoelectric properties is difficult due to the interdependency of the parameters. The interdependency among the parameters is represented by carrier concentration. Any favorable change in carrier concentration to improve electrical conductivity is accompanied by an unfavorable change in another property, such as increasing the electrical contribution for thermal conductivity and decreasing the Seebeck coefficient. Therefore, any optimization of the parameters should consider the carrier concentration [15]. The ideal thermoelectric material is called a "phonon glass electron crystal," which means it has low thermal conductivity as in glass and high electrical conductivity as in a well-ordered crystal. After a series of experiments, it was determined that heavily doped semiconductors are the most efficient bulk thermoelectric materials as they have the highest power factor together with low thermal conductivity [16]. Most of the studies in thermoelectricity and almost all commercial modules have focused on inorganic thermoelectric materials [3, 17] which includes skutterudites, clathrates, oxides, nitrides, pnicogens, half-Heusler alloys, Zintl-phase, and metal chalcogenide materials. Among inorganic materials, chalcogenides are considered the prime thermoelectric candidate and have been used extensively due to their reliability and better thermoelectric performance than other materials [7]. The term chalcogenide referred mainly to tellurides (Te), selenides (Se), and sulfides (S). Layered chalcogenides have a high figure of merit mainly because of their low thermal conductivity. Low thermal conductivity is attributed to the anisotropic crystal structure and strong lattice anharmonicity. Their relatively heavy atoms compared with other thermoelectric materials efficiently help to reduce thermal conductivity [2]. Layered chalcogenides could be easily formed into different types of structures. Moreover, their layered structure enables the modification and development of their properties at several levels using a variety of strategies. On the atomic scale, reduction of thermal conductivity by scattering phonons could be attained with the help of a layered structure by intercalation of guest atoms and layers between the host layers. Further, the low energy vibration of atoms could effectively scatter phonons. In the nanoscale, any stacking faults in the layered structure could result in a further reduction in lattice thermal conductivity, whereas in the microscale, the highly oriented microstructure improves the power factor by enhancing carriers' mobility in the in-plane directions [18].

3 Layered Chalcogenide Materials

Layered chalcogenides represent a massive group with multiple materials. In the following section we tried to classify layered materials into groups in which each group has certain common features between the members: (1) bismuth and antimony based materials which are known for their high performance near room temperature; (2) oxychalcogenides; (3) tin- and indium-based materials [19]; (4) homologous series; (5) layered sulfides, including titanium sulfides; and (6) ternary $ACrX_2$ layered struc-

tures [20]. The structure of chalcogenide materials is characterized by layers; the bonds in each layer are strong covalent bonds, which provides in-plane stability. The interaction that holds the layers together is van der Waals. According to the chemical bonding and anisotropic nature of the crystal structure, there is variation in thermoelectric properties with different crystallographic directions within the crystal [19]. Details of the structure of individual material and their thermoelectric properties and discussion of how the anisotropic nature of layered materials affects their thermoelectric properties are presented in the following sections.

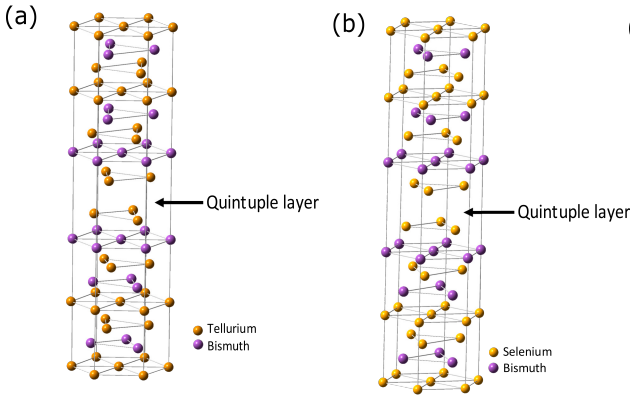

Figure 2: (a) Crystal structure of Bi_2Te_3 (b) Crystal structure of Bi_2Se_3.

3.1 Structure of Layered chalcogenide materials

3.1.1 Bismuth and Antimony-Based Layered Materials

In this section we included Bi and Sb telluride and selenide materials, whereas sulfides' compounds are excluded and discussed under the sulfide group. Although sulfur lies in the same group as Te and Se, however, bismuth sulfides adopt an orthorhombic structure different than rhombohedral structure adopted by bismuth tellurides and selenides. Sulfides show lower electrical conductivities compared to selenide and telluride because of their higher bandgap [21–23].

Bismuth telluride (Bi_2Te_3) is a narrow bandgap *n*-type semiconductor of (0.21 eV) and an indirect bandgap of 0.15 eV. Bismuth telluride has a distinctive rhombohedral layered crystal structure with five atoms in each unit cell forming quintuple layers of $Te_{(1)}$-Bi-$Te_{(2)}$-Bi-$Te_{(1)}$ stacked together by weak van der Waals forces along the *c*-axis as shown in Figure 2a. The Te atoms are presented in two different chemical states as the subscripts 1 and 2 show. However, within the layers, Bi-Te(2) atoms are bonded by a strong covalent bond, whereas Bi-Te(1) atoms are bonded by a covalent-ionic bond [2].

Since its discovery 60 years ago, bismuth telluride was first used by Goldsmith as an effective material for refrigeration purposes. It has been used as the most promising thermoelectric material with a high figure of merit (1.14) near room temperature (200–400 K) [22]. Because of the weak van der Waals bonds between layers, Bi_2Te_3 exhibits high thermoelectric properties and demonstrates easy cleavage along the (001) plane [2].

Bismuth selenide (Bi_2Se_3) is a narrow bandgap (0.3 eV) *n*-type semiconductor. Analogous to bismuth telluride, it has a rhombohedral anisotropic layered structure with quintuple layers and five atoms in each unit cell [22]. The two Bi atoms and three Se atoms are packed similar to Bi_2Te_3 pattern Se(1)–Bi–Se(2)–Bi–Se(1) with weak van der Waals bonds between neighboring Se(1) planes as shown in Figure 2b. Compared with bismuth telluride, bismuth selenide possesses high thermal conductivity because of the light atomic weight of Se. Therefore, the thermoelectric performance of $Bi_2Te_3$is much better than Bi_2Se_3 [2].

Antimony telluride (Sb_2Te_3) is a layered rhombohedral crystal structure *p*-type semiconductor. Its unit cell consists of five atoms packed with a similar Bi_2Te_3 and Bi_2Se_3 pattern, Te(1)-Sb-Te(2)-Sb-Te(1). The layers are connected by weak van der Waals bonds, so the cleavage is apt to occur perpendicular to the *c*-axis (cross-plane direction). As an intrinsic semiconductor, Sb_2Te_3 has attracted attention for its high electrical conductivity and low thermal conductivity. It is the leading material for thermoelectric applications near room temperature (300–500 K) [24].

3.1.2 Oxychalecognide Materials

Layered oxychalcogenides thermoelectric materials have gained considerable attention due to their intrinsically low thermal conductivity, moderate Seebeck coefficient and tunable electrical conductivity [25].

The Bi-O-X system is a group of oxy-layered materials that has a complex tetragonal structure. One example is Bi_2O_2Se, which consists of tetragonal $(BiO)_n$ layers with Se atoms occupying interlayer positions as shown in Figure 3. Due to the strong electronegativity of oxygen atoms, oxychalcogen systems suffer from low electrical conductivity. However, they exhibit a moderate Seebeck coefficient.

BiCuOCh (Ch = S, Se, Te) is a group of oxychalcogenides that have the structure of space group = *P4/nmm* and consist of alternately stacked $(Bi_2O_2)^{+2}$ insulating lay-

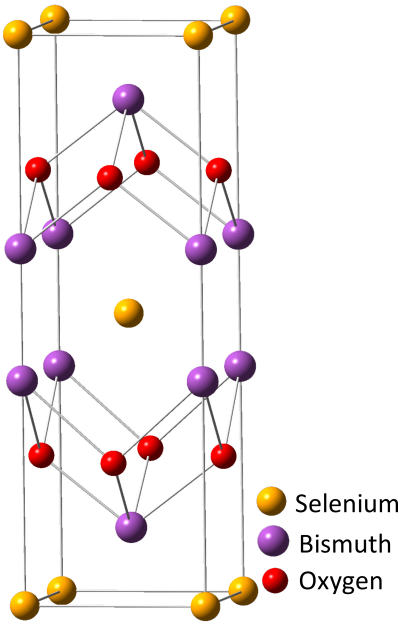

Figure 3: Crystal structure of Bi_2O_2Se.

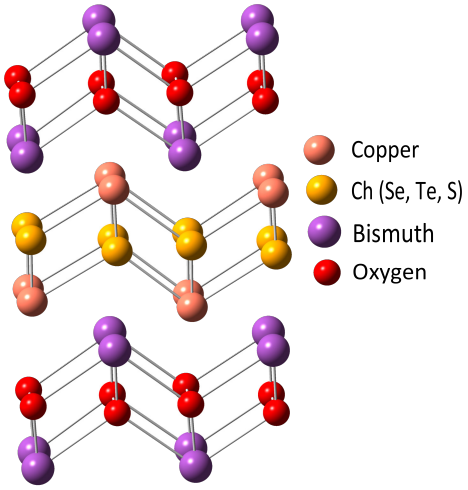

Figure 4: Crystal structure of BiCuOCh (Ch = S, Se, Te).

ers and $(Cu_2Ch_2)^{-2}$ conducting layers as shown in Figure 4. They exhibit extremely low thermal conductivity and have poor electrical conductivity due to low carrier mobility. BiCuOSe was recently reported as a promising thermoelectric material for its high *ZT* (> 0.8) at a high- temperature range (923 K). It is a *p*-type material composed of alternating insulating $(Bi_2O_2)^{2+}$ layers with conductive $(Cu_2Se_2)^{2-}$. The thermoelectric measurements suggest that the electrical properties of BiCuSe is lower than other thermoelectric systems; thus the high thermoelectric performance of BiCuSe originates from its very low thermal conductivity instead of its power factor [26–28]. Compared with BiCuSeO, BiCuOTe has a higher power factor as it has a better hole mobility attributed to the antibonding between Cu and Te compared with antibonding between Cu and Se. Therefore hole mobility can be improved significantly in BiCuSeTe compared with BiCuSeO [26].

3.1.3 Homologous Series

Homologous layered materials are an interesting class of thermoelectric materials that are built on the same structure of a certain model and can be expanded by regular increments in different directions [18, 22]. Examples of homologous thermoelectric series are $CsBi_4Te_6$, a member of the $Cs_4[Bi_{2n}+4Te_{3n}+6]$ homologous series, and $Pb_5Bi_6Se_{14}$, a member of the cannizzarite homologous series.

$CsBi_4Te_6$ is a *p*-type semiconductor with a narrow bandgap of (0.1 eV), which is nearly half the value compared with Bi_2Te_3. It has an anisotropic layered structure with Bi_4Te_6 slabs interconnected by Bi-Bi bonds parallel to the *b*-axis and altered with Cs^+ ionic layers as shown in Figure 5a. $CsBi_4Te_6$ is a potential candidate for thermoelectric application and exhibits a high figure of merit of 0.8 at low temperatures, which is attributed mainly to the narrow bandgap [18, 22].

$Pb_5Bi_6Se_{14}$ is an *n*-type semiconductor. Its crystal structure consists of infinite alternating PbSe- and Bi_2Se_3-type layers along the *c*-axis, forming a three-dimensional structure, as shown in Figure 5b. The interfaces between the PbSe and Bi_2Se_3 layers scatter phonons as well as charge carriers, leading to a highly anisotropic electrical mobility and lattice thermal conductivity between in- and cross-plane directions. Electrical conductivity is much higher in-plane direction than cross-plane direction, whereas lattice thermal conductivity is slightly higher for the in-plane direction than for the cross-plane direction. However, the Seebeck coefficient is insensitive to the crystal orientation and exhibits nearly similar values for both in- and cross-plane directions. As a result, a higher *ZT* of 0.46 has been achieved for the in-plane direction at 75 K. The thermoelectric properties of homologous compounds can be controlled by modifying the shape and size of the structural module. Therefore, homologous materials are a suitable platform for developing new thermoelectric materials [18].

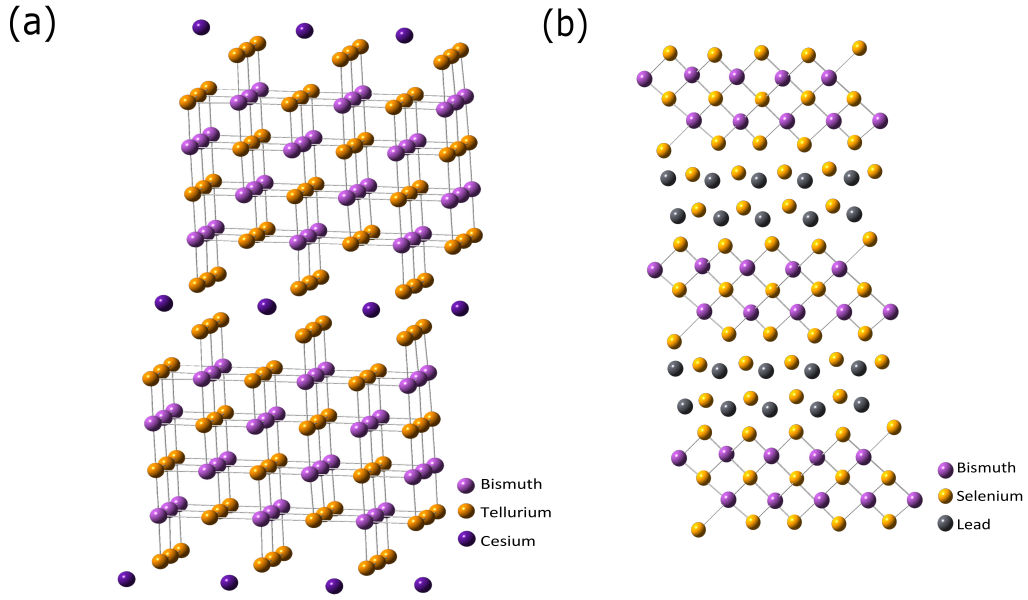

Figure 5: (a) Crystal structure of $CsBi_4Te_6$. (b) Crystal structures of $Pb_5Bi_6Se_{14}$.

3.1.4 Sn- and In-Based Layered Materials

Sn- and In-based systems are typical thermoelectric materials with low cost and good thermoelectric performance. Tin selenide (SnSe) is a *p*-type semiconductor with simple orthorhombic, layered-structure material with a zigzag accordion chain along the *b*-axis and a bandgap of 0.86 eV. Each layer consists of two-atom-thick slabs (Se and Sn) along the in-plane direction, with strong Sn-Se bonds within the layer and weak Sn-Se bonds between layers along the cross-plane direction, as shown in Figure 6a. At a temperature of 800 K, tin selenide undergoes reversible transition distortion from the orthorhombic low-temperature *Pnma* space group to the orthorhombic high-temperature *Cmcm* space group. At this transition temperature, the power factor reaches its maximum value as the *Cmcm* phase exhibits a reduction in energy with enhancement in carrier mobility while preserving the low thermal conductivity [15, 29]. Similarly, In_4Se_3 forms a layered crystal structure of $(In_3)^{+5}$ clusters covalently bonded to Se ions in the in-plane. Along the cross-plane direction, the planes are held together by van der Waals interactions as shown in Figure 6b. Tin selenide is a *p*-type semiconductor with a relatively low carrier density of 10^{17}–10^{18} cm^{-3}. At room temperature, it possesses a high electrical resistivity of 10–10^5 Ωcm. Even with high electrical resistivity, the obtained power factors of SnSe crystals are moderate at high temperatures as the crystals possess a high Seebeck coefficient and are much higher than other materials with low intrinsic thermal conductivity [29, 30]. Because of the high electrical resistivity, tin selenide was ignored by thermoelectric researchers for a long time [31], until Sassi, S, *et al.* reported a high *ZT* of 2.6 for a single crystal along the *b*-axis, 2.3 along the *c*-axis, and 0.8 along cross the plane direction (*a*-axis) [15].

SnS recently has attracted interest as it has the same structure and chemical bond of tin selenide, as shown in Figure 6c. It is *p*-type semiconductor, environmentally

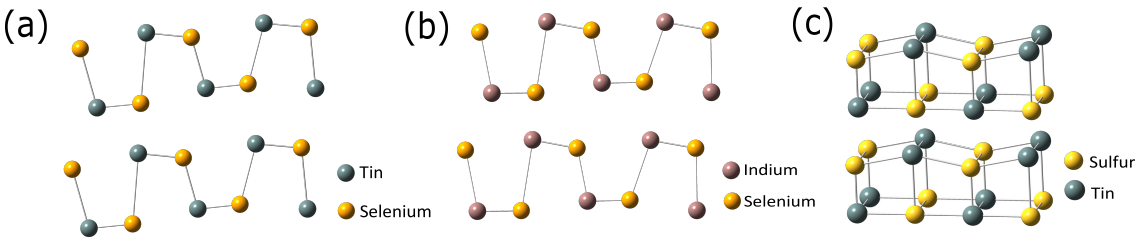

Figure 6: Crystal structure of (a) SnSe, (b) InSe, and (c) SnS.

friendly and cost-effective, and its resources are earth-abundant. Similar to SnSe, SnS possesses extremely low thermal conductivity (below 1 $Wm^{-1}K^{-1}$) with a high Seebeck coefficient, which makes it a promising material for thermoelectric application [32].

3.1.5 Layered sulfides

Multiple Sulfides materials have been discovered over the past 10 years and have proven their efficiency as environmentally friendly thermoelectric materials. TiS_2 is a misfit-layered sulfide that has a layered crystal structure connected by van der Waals forces along the cross-plane direction. TiS_2 has a wide range of chemical compositions with different concentrations of Ti atoms ranging from stoichiometric up to $1+x$, where $0 \leq x < 1$. The excess Ti atoms occupy the places between layers because they are weakly bonded. TiS_2 is considered an efficient *n*-type material for thermoelectric applications as it is composed of light, low-toxic, and earth-abundant elements. TiS_2 shows the best performance at high temperatures for both single as well as polycrystalline forms. The TiS_2 single-crystal possesses a high power factor; however, its *ZT* is limited to ~0.16 at 300 K because of the high lattice thermal conductivity [18]. Therefore, the intercalation of the other layers, such as PbS, BiS, and Sn, has been found to be an effective way of reducing its thermal conductivity. Figure 7a shows a TiS_2 compound structure with the structure of other materials intercalated between its layers [33].

Misfit layered sulfides are a large layered material group with a general formula $[MS]_{1+m}[TS_2]_n$, where M = Sn, Pb, Sb, Bi, or rare-earth metals; T = Ti, V, Cr, Nb, and Ta; and n = 1, 2, 3 [34] and 0.08 <m <0.28. These materials consist of alternating layers of MS and TS_2 where the TS_2 layer provides the electron path way and thermopower whereas the intercalated MS layer suppresses the transport of phonons [35]. The crystal structure and physical properties of this misfit family were studied extensively in the 1990s, however, not many reports on their thermoelectric properties exist to date. The crystal structure of $[LaS]_{1.14}NbS_2$ is shown in Figure 7b as an example. Recently, misfit-layered sulfides have gained interest in thermoelectric research for their good thermoelectric behavior, where the intercalated NaCl-type MS layer is primarily responsible for the disorder (reduction in κ_{lat}) and the CdI_2-type TS_2 layer behaves as a charge-carrier pathway [18]. The entire crystal structure is stabilized through charge transfer from the MS layer to the TS_2 layer. Wan *et al.* [33] studied a series of *n*-type $(MS)_{1+x}(TiS_2)_2$ (*M = Pb, Bi, Sn*) misfit layer compounds and found that they exhibit very low thermal conductivity due to the weak interlayer bond. The figure of merit values of these compounds were found to range between 0.28 and 0.37 at 700 K with a maximum *ZT* of 0.37 for $(SnS)_{1.2}(TiS_2)_2$. Their ZT is affected by the microstructure due to the anisotropic nature in the atomic bonds of the misfit layered compounds [18]. Therefore, tuning its microstructure, which is mainly affected by its synthesis, is one strategy to enhance its *ZT*. Jood *et al.* [34] prepared misfit-layered *n*-type $(LaS)_{1.2}CrS_2$ and *p*-type $(LaS)_{1.14}$ NbS_2 by CS_2 sulfurization for 6 and 12 hours followed by the pressure-assisted consolidation to produce randomly and highly oriented samples whose microstructures were tunable. A highly oriented texture sample pro-

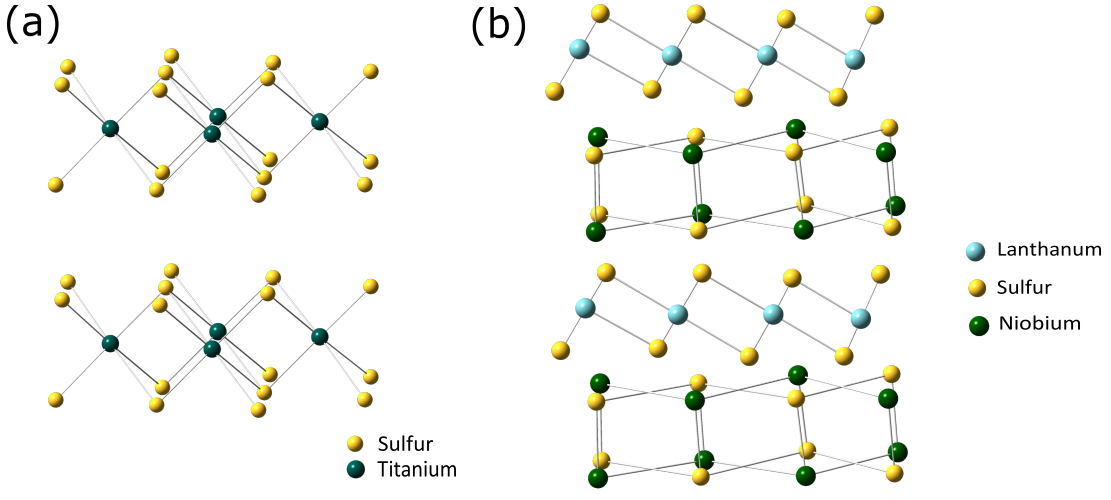

Figure 7: Crystal structures of (a) TiS_2 and (b) $[LaS]_{1.14}NbS_2$.

duced the highest *ZT* of 0.14 at 950 K among $(LaS)_{1.2}CrS_2$ systems, while the weakly oriented texture produced the highest *ZT* of 0.15 at 950 K among $(LaS)_{1.14}NbS_2$.

Recently, a new class of *n*-type layered sulfide materials ($MnBi_4S_7$ and $FeBi_4S_7$) has been reported. They exhibit a complex, monoclinic, low-symmetry layered structure shown in Figure 8. The complex structure and the presence of lone pair electrons with Bi^{+2} are the main reasons for the low thermal conductivity of these materials. In addition, they have a relatively high power factor making these materials good candidates for low and intermediate-temperature thermoelectric applications [36].

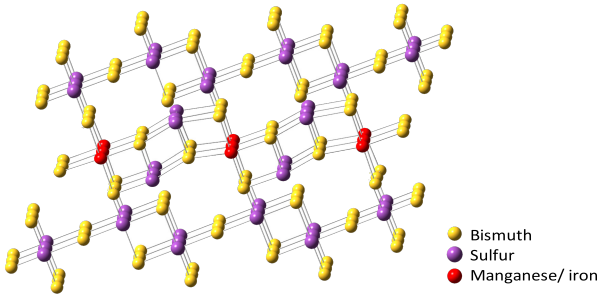

Figure 8: Crystal structure of $MnBi_4S_7$ and $FeBi_4S_7$.

Bismuth sulfide (Bi_2S_3) has received interest for use in thermoelectric applications due to the high abundance of sulfur on earth [37]. It is *n*-type material that crystallizes in a highly anisotropic orthorhombic structure with a space group *Pnma* that contains 20 atoms per unit cell. It has a wide direct bandgap of 1.3 eV; thus it has low electrical conductivity in pristine form and has a low *ZT* value [20, 38, 39].

BiS_2-based compounds show relatively high thermoelectric performance. Their crystal structure is composed of a BiS_2-conducting layer stacked alternately with an insulating layer. An example of BiS_2-based thermoelectric compounds is $SrFBiS_2$. $SrFBiS_2$ is an *n*-type material that belongs to the tetragonal *P4/nmm* space group, and its structure is built up by stacking alternately a SrF layer with NaCl-type BiS_2 layer, as shown in Figure 9. $SrFBiS_2$ has low thermal conductivity with a relatively high power factor at low temperatures. $SrFBiS_2$ is expected to be a parent for a group of material by doping it with different materials. Doping is a achieved by substituting Sr^{+2} site with rare-earth metal (RE^{+3}) [40, 41].

$AgBi_3S_5$ is a new nontoxic *n*-type thermoelectric material with high thermoelectric performance. It has a complex structure composed of NaCl-type fragments [21]. It has very low thermal conductivity in the temperature range of

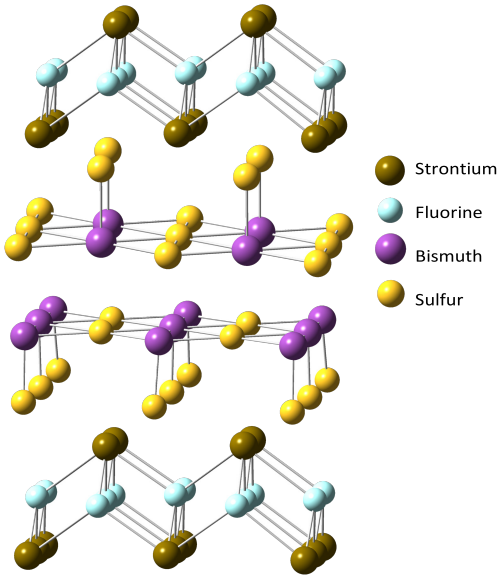

Figure 9: Crystal structure of $SrFBiS_2$.

300-800 K due to the unusual vibrational properties associated with Ag and Bi atoms [42].

3.1.6 Ternary ACrX2-Layered Structures

$ACrX_2$-layered compounds, where A represents Ni, Cu, or Ag and X represents S or Se, are a group of magnetic materials that exhibit good thermoelectric performance at low to moderate temperatures [23]. $ACrX_2$ compounds possess a trigonal-layered structure (R3m), where Cr^{+3} cations are in distorted octahedral coordination to the X^{-2} anions, and A atoms (Ag or Cu) fill the interlayer spaces and occupy tetrahedral sites, as shown in Figure 10. Within the layer, the atoms of CrX_2 are bounded by strong ionic bonds, while the bonds are weak van der Waals between the neighboring triple layers. The thermoelectric performance of this group depends strongly on their synthesis. A highly textured *p*-type $CuCrS_2$ sample with high electrical conductivity has been obtained via a specific heat treatment process, whereas the same sample fabricated by ball milling and spark plasma sintering methods exhibited poor thermoelectric performance with a *ZT* of 0.11. A maximum *ZT* of 2 at 300 K and 1 at 848 K was reported by Tewari *et al.* and Gascoin *et al.* [43, 44] for $CuCrS_2$ and $AgCrS_2$, respectively. A *ZT* of 1.4 was achieved in sandwich-like *p*-type $(AgCrSe_2)_{0.5}(CuCrSe_2)_{0.5}$ at 773 K [45].

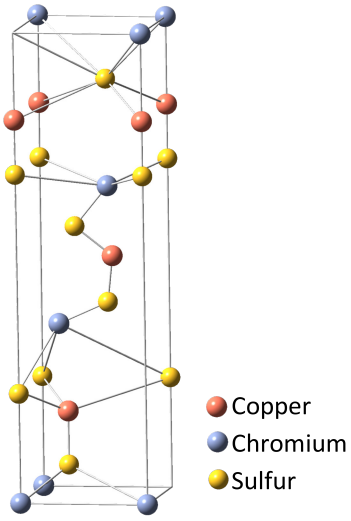

Figure 10: Crystal structures of $CuCrS_2$.

3.2 Anisotropy

Due to the layered crystal structure of layered chalcogenide materials, the materials exhibit a significant anisotropic structure and properties of in-plane direction versus cross-plane direction. In a single crystal, the lamellar structure leads to an easy cleavage of planes that are perpendicular to the cross-plane direction. The atomic interactions within the plane are characterized by covalent bonds and the layers are held by weak van der Waals bonds along the cross-plane direction. The difference in the nature of the atomic bonds in various directions results in anisotropy in thermoelectric properties when measured in different directions. Thermal and electrical conductivity, in most of the materials, are much lower in the cross-plane than within the plane direction [46]. This is attributed mainly to weak van der Waals interactions between the planes. The weak bonds act as a thermal and electrical boundary that heavily scatter phonons and electrons [47]. In several studies, the Seebeck coefficient was found to be isotropic and independent of the crystallographic direction [46, 48–51]. However, in some other studies [34, 52], the Seebeck coefficient exhibit anisotropy in different directions. Zhao *et al.* [50] reported on the thermoelectric performance of a SnSe single crystal with significant anisotropy in different directions. They reported ultrahigh *ZT* equals 2.6 in the b direction (within the plane), and a high *ZT* equals 2.3 in the c direction (which is in-plane direction, perpendicular to b but in the same plane). They reported a significantly reduced *ZT* of 0.8 across the plane direction (perpendicular to the bc plane). Similarly, thermal and electrical conductivities have been found to be two and four times higher for the in-plane direction than the cross-plane direction in an *n*-type $Bi_2(Te_{1-x}Se_x)_3$ single crystal, whereas no significant difference in the Seebeck coefficient has been reported. In total, *ZT* has been found to be two times higher within the plane direction than in the cross-plane direction [48]. In polycrystalline and nanostructured materials, it has been found that for the crystals, the grains tend to be oriented in a significant preferential orientation due to the lamellar structure when they are pressed or sintered, whereas the nanostructured material parts tend to grow in a preferred direction. The anisotropic nature of the bonds, where intralayer covalent bonds are stronger than interlayer covalent bonds, led grains to grow perpendicular to the applied pressure [34, 53]. Hence, they exhibit anisotropic thermoelectric properties in the direction of pressing that is not perpendicular. Bi_2S_3 has a lamellar structure that forms a long chain parallel to the (001) direction. The XRD pattern of the prepared Bi_2S_3 nanoribbon proved the anisotropic structure and the tendency of the ribbon to grow along the preferential (001) direction [54]. Based on the XRD pattern for the surface of the several sintered pellets of $(MS)_{1+x}(TiS_2)_2$ materials, Wan *et al.* [33] reported that the crystals preferred to align perpendicular to the pressing direction as they observed sharp (00l) peaks, which represent the planes perpendicular to the pressing direction; very few (h k l) planes were detected, as seen in Figure 11. The degree of orientation of the planes is high so that the thermoelectric properties of the polycrystalline samples approach the values of the properties reported for in-plane single crystals for the same materials. Chere *et al.* [51] found that the grains in the

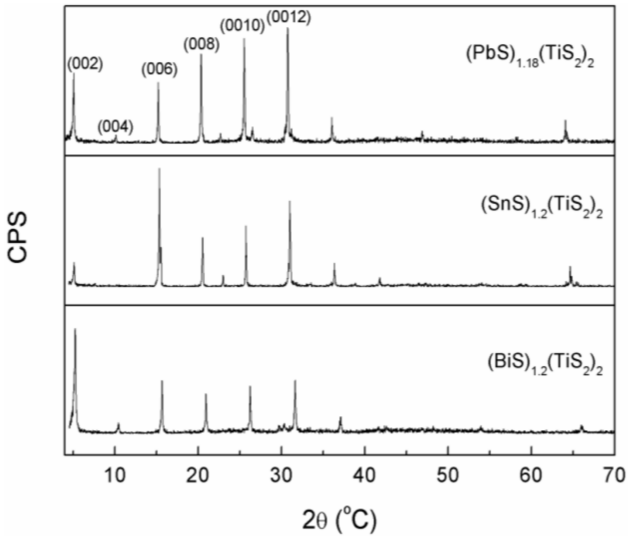

Figure 11: XRD patterns of $(BiS)_{1.2}(TiS_2)_2$, $(SnS)_{1.2}(TiS_2)_2$ and $(PbS)_{1.18}(TiS_2)_2$. Reproduced from Ref. [33].

p-type SnSe polycrystalline material grew preferentially along the (400) and (111) planes. Therefore, anisotropic thermoelectric properties have been observed. Electrical conductivity was very high when measured perpendicular to the press direction, but thermal conductivity was much lower along the pressing direction leading to higher *ZT* along the pressing direction. Sassi *et al.* [53] reported anisotropic thermoelectric properties in homologous *n*-type $Pb_5Bi_6Se_{14-0.25}I_{0.25}$. A bar-shaped compressed sample was cut in parallel and perpendicular directions to the pressing direction, and thermoelectric properties were measured in both directions. *ZT* was calculated to be 0.5 in the perpendicular direction and about 0.35 in the parallel direction. In another study, Xu *et al.* [49] found that the electrical conductivity of *n*-type $SnSe_2$ is about two times higher in-plane direction than in the cross-plane direction, whereas thermal conductivity is about twice or three times higher. In another study [34], the XRD pattern of the surface perpendicular to the pressing direction of the *n*-type $(LaS)_{1.2}CrS_2$ and $(LaS)_{1.14}NbS_2$ compacted samples show that the crystals are oriented along the (001) planes. Highly anisotropic thermal and electrical properties have been

Table 1: Layered chalcogenide materials with their *ZT* values.

Material	Type	ZT	T,K	Reference
Bi_2Te_3	n	0.4	300	[55]
Bi_2Se_3	n	0.75	423	[56]
$Ti_{1.008}S_2$	n	0.12	300	[57]
$Cu_{0.1}TiS_2$	n	0.5	800	[58]
$(BiS)_{1.2}(TiS_2)_2$	n	0.28	700	[33]
$(BiS)_{1.2}(TiS_2)_2$	n	0.24	750	[59]
$(SnS)_{1.2}(TiS_2)_2$	n	0.37	700	[59]
$(PbS)_{1.18}(TiS_2)_2$	n	0.28	700	[59]
$(SnS)_{1.2}(TiS_2)_2$	n	0.37	673	[60]
$(Yb_2S_2)_{0.62}NbS_2$	p	0.1	300	[61]
$(LaS)_{1.14}NbS_2$	p	0.02	300	[34]
		0.15	950	
$(LaS)_{1.2}CrS_2$	n	0.12	950	[34]
$MnBi_4S_7$	n	0.21	700	[36]
$FeBi_4S_7$	n	0.19	600	[36]
Bi_2S_3	n	0.08	773	[39]
$Pb_5Bi_6Se_{14}$	n	0.01	300	[62]
$Pb_5Bi_{12}Se_{23}$	n	0.01	300	[62]
$Pb_5Bi18Se_{32}$	n	0.03	300	[62]
SnSe (single crystal)	p	2.62 (*b*-axis)	923	[15]
SnSe	p	0.5	820	[15]
SnS	p	0.41	848	[32]
InSe	n	0.525	600	[63]
In_4Se_3	n	0.6	700	[64]
$AgCrSe_2$	p	1	848	[44]
$CuCrS_2$	p	0.9	350	[65]
$CuCrSe_2$	p	0.17	300	[43]
$NiCr_2S_4$	n	0.024	313	[66]
Bi_2O_2Se	n	0.2	800	[67]
$Bi_4O_4S_3$	n	0.03	300	[68]
$Bi_{1.9}O_2Se$	n	0.12	773	[69]
BiCuSeO	p	0.5	650	[70]
$BiCu_{0.975}SeO$	p	0.81	650	[70]
BiCuOTe	p	0.51	600	[26]
BiCuOS	p	0.07	650	[71]

observed in the in-plane and cross-plane directions. For example, electrical resistivity was ~170 and 280 μΩ m at 950 K for in-plane and cross-plane directions, respectively. This is mainly because the oriented texture allows higher mobility of carriers within the plane, whereas scattering them at the interfaces between the layers. Similarly, thermal conductivity is lower in the cross-plane than in the in-plane direction because the interfaces scatter phonons. The large grains reduce the number of phonons scattered at grain boundaries.

Grain alignment in a preferred orientation in polycrystalline materials has been found to be effective in enhancing the *ZT* by enhancing the power factor in the in-plane direction. However, in several studies [34, 46] where polycrystalline materials were prepared in nanograin forms, it was found that the grains are randomly oriented, and in turn, there was no significant improvement in *ZT* after nanostructuring. Although nanostructuring has a significant effect on reducing thermal conductivity, the randomness in grains orientation has a negative impact on the power factor, which in turn does not show any enhancement in total *ZT*. Therefore, it is a challenge to keep small grains with partial alignment to improve the power factor to a level close to that of a single crystal while keeping the fine grain to reduce thermal conductivity. Yan *et al.* [46] achieved partial grain alignment in *n*-type $Bi_2Te_{2.7}Se_{0.3}$ by repressing the pressed samples with a larger diameter die at a higher temperature. By this way, small grains were forced to be aligned in-plane perpendicular to the pressing direction. They reported an enhancement in *ZT* from 0.85 for random grains to 1.04 after partial alignment of grains perpendicular to the press direction. Although *ZT* along the pressing direction decreased, this will not be considered because only the direction of high *ZT* is used in thermoelectric devices. Jood *et al.* [34] reported the effect of the degree of orientation on thermoelectric properties of *n*-type $(LaS)_{1.20}CrS_2$ and *p*-type $(LaS)_{1.14}NbS_2$ materials. They prepared highly oriented and randomly oriented microstructure samples of both materials. They found that both highly and randomly oriented samples of $(LaS)_{1.20}CrS_2$ material provide ultralow thermal conductivity perpendicular to the pressing direction. The highly oriented texture provides higher electrical conductivity, which results in a higher power factor and higher *ZT* in the in-plane direction in both samples. Similar to $(LaS)_{1.20}CrS_2$, the power factor of the oriented $(LaS)_{1.14}NbS_2$ sample was higher (22%) than the random texture in the in-plane direction as a result of higher Seebeck coefficient and higher electrical conductivity. However, it possesses higher thermal conductivity, which was 40% higher in the oriented sample than the random one, which overcomes the increment in power factor and leads to a lower ZT in the oriented sample. Table 1 illustrates examples of layered chalcogenide materials with their *ZT* at different temperatures.

4 Strategies for Improving Thermoelectric Performance

Traditional thermoelectric materials did not possess ideal thermoelectric properties. Designing and optimizing thermoelectric materials with high efficiency is a complex and challenging task. It is believed that the best thermoelectric materials provide amorphous phonon glass to achieve glass-like lattice low thermal conductivity with crystal electronic structure where electrons have high electric conductivity. The phonon glass region is suitable for hosting disorders and doping for blocking phonons without affecting the carrier mobility in the electron crystal region. Researchers have searched for thermoelectric materials that have a complex crystal structure and large molecular weight [29]. Skutterides and clathrates are, for example, cage-like materials with voids that could be occupied by foreign atoms. The inserted atoms have the ability to rattle in the cage and result in scattering the phonons and enhancing lattice thermal conductivity [72]. Layered chalcogenide materials possess low thermal conductivity because of their intrinsic lattice anharmonicity [73], which is measured by the Gruneisen parameter. The Gruneisen parameter is an indication of how much phonon vibrations are deviated from harmonic oscillation in crystal lattice. Anharmonicity of the chemical bonds plays an important role in limiting the lattice thermal conductivity [28, 74]. In addition, layered chalcogenides possess low thermal conductivity in the cross-plane direction because of the weak van der Waals interactions (soft bonds) between the layers; however, for those materials to be widely used in commercial applications, further reduction of thermal conductivity is still required. Besides, the Seebeck coefficient and electrical conductivity must be improved [22]. Several strategies have been followed with the aim of decoupling the parameters and attaining a high power factor, low thermal conductivity, or a combination of both. Improving the power factor can be attained by appropriate carrier doping, quantum confinement, energy carrier filtering, lowering the effective mass, and modifying the band structure by alloying [30, 75]. Thermal conductivity could be reduced by adding interfaces in order to intensify phonon scattering at the atomic, nanoscale, and microscale by forming solid solutions (alloying), nanostructuring, or all-scale hierarchi-

cal architecturing [30, 75]. It is worth noting that the evolution of thermoelectric properties is not limited to the use of only one method. More than one method has been utilized simultaneously in several studies to attain the highest improvement in thermoelectric performance. Methods for improving thermoelectric performance include doping, nanostructuring, and nanocompositing.

4.1 Doping

Adjusting the carrier concentration shows the best improved thermoelectric effect in semiconductors. Heavily doped semiconductors are the best thermoelectric materials with a greater power factor than the undoped counterpart [3, 76]. Dopant additions have been shown to have a significant impact on the electron density distribution in thermoelectric chalcogenides [59, 77]. Moreover, doping can play an important role in reducing the lattice thermal conductivity by creating defects and scattering phonons. However, the doping level should be optimized to a certain limit in a way that increases electrical conductivity and does not affect the Seebeck coefficient [3, 7, 78]. Wei *et al.* [79] studied the effect of Na, Li, and K doping with *p*-type SnSe. The results showed that Na is the most efficient dopant. The addition of 1% Na to SnSe increased the carrier concentration, which led to a maximum *ZT* of 0.8. In this study, the dopant atoms disturb the pseudopotential of the lattice and act as scattering centers for the carriers, which in turn affect the carrier's mobility. The difference in size between the matrix atoms and the dopant leads to an extra scattering of carriers. As the difference of radius increases (in case of Li^+ and K^+), more scattering of the carriers is expected. This is likely the reason why the mobility of carriers decreases more than Na and Ag.

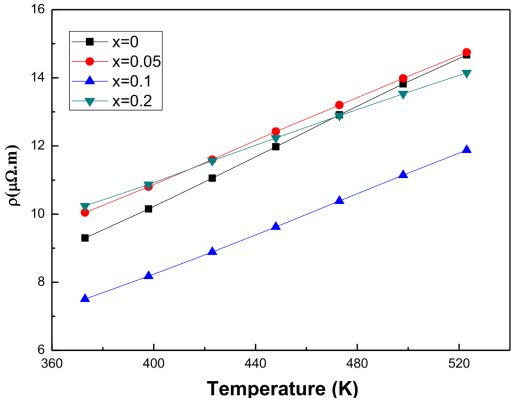

Figure 12: Electrical resistivity of In-doped Bi_2Te_3 bulk samples versus temperature. Reproduced from Ref. [84].

Silver has been found to be an effective dopant compared with Na when added to SnSe because of its high solubility when subjected to repeated heating and cooling. According to these results, Ag was able to increase the carrier concentration to 9×10^{18} cm^{-3}, leading to an improvement of the electrical conductivity and power factor [80, 81]. However, similar to the previous study, the mobility of the doped sample has been found to be much lower than the pristine sample (12 cm^2 V^{-1} s^{-1} and 7 cm^2 V^{-1} s^{-1} for pristine and 5% Ag- doped SnSe, respectively), which suggest that Ag atoms scattering the carriers. In another study [77], it was found that doping *n*-type SnSe with $PbBr_2$ led to a significant improvement in carrier concentration whereas the carrier mobility is affected negatively by increasing carrier concentration. Overall, electrical conductivity was found to be higher for the first addition of 1% and 2% $PbBr_2$ than those of 3% and 4% which is due to decrease of the mobility after scattering of the carriers. However, doping with 3% $PbBr_2$ lead to an enhancement of *ZT* to 0.54 at 793 K. Zhang *et al.* [82] studied the effect of several dopings of *p*-type SnTe and found that 0.25 atom% In-doped SnTe improved the Seebeck coefficient significantly and increases *ZT* to 1.1 at 873 K. However, electrical conductivity was found to decrease with doping due to the reduction of carrier mobility, which indicates that dopants affect the carriers' mobility. In addition to the improvement in electrical conductivity, ultralow thermal conductivity has been achieved when doping *p*-type SnSe with 0.01 Cu, leading to a total improvement of *ZT* to 1.2 at 873 K [83]. The enhanced electrical conductivity is attributed to the high carrier concentration induced by Cu dopants, whereas the presence of Cu atoms plays an important role as scattering centers for the phonon. A significant reduction in the lattice thermal conductivity, which led to a measurable improvement in *ZT*, was reported by Putri *et al.* [59], who used chromium as a dopant for *n*-type $(BiS)_{1.2}(TiS_2)_2$ misfit layer compound. The calculated *ZT* values for doped samples with different doping amounts ($x = 0.025$, $x = 0.05$, $x = 0.1$) exhibit an increase in *ZT* to 0.24–0.3. The main contribution for chromium doping in this study corresponds to its role in reducing total thermal conductivity. Indium has been added to Bi_2Te_3, and a maximum *ZT* of 1.1 was achieved at 448 K [84]. The enhancement was attributed to an effective increase of electrical conductivity because of high carrier concentration and a reduction of thermal conductivity due to phonon scattering. In this study, several amounts of In were added; however, In with $x = 0.1$ exhibited the best thermoelectric behavior. Although doping increases the carrier concentration, which contributes

Table 2: *ZT* of doped layered chalcogenide materials.

Material	Dopant	Type	ZT	T, K	Reference
Bi_2Te_3	Pb (0.3 at%)	n	-	473	[78]
$Bi_{0.5}Sb_{1.5}Te_3$	Sb	p	1.3	380	[86]
$BiSb_2Te_3$	In	p	1.4	500	[85]
Bi_2Te_3	In (1%)	p	0.65	385	[93]
Bi_2Te_3	Ce	n	1.29	398	[94]
Bi_2Te_3	I (0.1 %)	n	1.1	448	[84]
Bi_2Te_3	Cr (1%)	p	0.8	325	[95]
Bi_2Te_3	Cu	n	1.09	336	[96]
Bi_2Te_3	Ge	p	0.95	298	[97]
$Bi2Te_{1.9}Se_{1.1}$	SbI_3	n	1.1	600	[98]
$Bi_{0.5}Sb_{1.5}Te_3$	Cu	p	1.17	530	[99]
$Bi_{0.5}Sb_{1.5}Te_3$	Mn	p	1.3	430	[100]
Sb_2Te_3	Sulfur	p	0.95	423	[101]
TiS_2	Co (0.3)	n	0.03	310	[102]
TiS_2	Cu (0.02)	n	0.45	800	[103]
TiS_2	Sn	n	0.46	623	[104]
$TiS_{1.5}Se_{0.5}$	Cu (0.05)	n	0.54	700	[105]
$(BiS)_{1.2}(TiS_2)_2$	Cr (0.025)	n	0.3	750	[59]
$(SnS)_{1.2}(TiS_2)_2$	Cu	-	0.42	720	[106]
Bi_2S_3	$BiCl_3$	n	0.6	760	[19]
Bi_2S_3	$CuBr_2$	n	0.72	773	[38]
Bi_2Se_3	Te (1.5%)	n	0.67	473	[107]
Bi_2Se_3	Cu (0.1)	n	0.54	590	[108]
Bi_2Se_3	Ni	n	0.1	298	[109]
Bi_2O_2Se	Ag	n	0.072	673	[110]
Bi_2O_2Se	Cl	n	0.23	823	[111]
Bi_2O_2Se	Ge	n	0.25	723	[112]
Bi_2O_2Se	Ge	n	0.3	823	[113]
BiCuSeO	Sr	p	-	300	[27]
BiCuSeO	Sr	p	0.76	873	[114]
BiCuSeO	Ba	P	1.1	923	[115]
BiCuSeO	Mg	p	0.67	923	[116]
BiCuSeO	Ca	p	0.9	923	[28]
BiCuSeO	Na	p	0.91	923	[117]
BiCuSeO	Zn	p	0.65	873	[118]
BiCuSeO	Sn	p	1.09	773	[119]
BiCuSeO	Pb	p	1.14	823	[120]
BiCuSeO	Sm	p	0.74	873	[121]
BiCuOTe	K	p	0.69	700	[122]
$AgBi_3S_5$	Cl	n	1	800	[42]
$CsBi_4Te_6$	SbI_3 (0.05)	p		184	[123]
$CsBi_4Te_6$	SbI_3 (0.06%)	p	0.8	225	[124]
$Pb_5Bi_6Se_{14}$	I	n	0.5	700	[53]
$Pb_5Bi_6Se_{14}$	Te	n	0.5	723	[125]
SnSe	Na (1%)	p	0.8	800	[79]
SnSe	K	p	0.8	800	[79]
SnSe	Na (1.5 at.%)	p	0.8	773	[51]
SnSe	(0.5% Na +0.5% K)	p	1.2	773	[126]

Table 2: ... continued

Material	Dopant	Type	ZT	T, K	Reference
SnSe	Zn	p	0.96	873	[127]
SnSe	Ag	p	0.6	750	[80, 81]
SnSe	Sm	p	0.55	823	[128]
SnSe	I	n	0.8	773	[129]
SnSe	$BiCl_3$	n	0.7	793	[130]
SnSe	Bi	n	2.2	773	[75]
SnSe	$PbBr_2$	n	0.54	739	[77]
SnSe	$LaCl_3$	p	0.55	750	[131]
SnSe	Br	n	1.3	773	[132]
SnSe	Ge	p	0.6	823	[133]
SnSe	Ge	p	0.77	800	[134]
SnSe	Cu	p	1.2	873	[83]
SnSe	Cu	p	0.7	773	[135]
SnTe	In (0.25 at%)	p	1.1	873	[82]
SnTe	Ca&In	p	1.65	840	[136]
SnS	Ag	p	0.6	873	[81]
SnS	Na	p	0.65	800	[137]
SnS	Na	p	1.1	870	[138]
InSnTe	Al (0.1)	p	0.28	668	[139]
In_2Se	Sn (0.05)	p	0.66	700	[140]
In_4Se_3	Cl (0.03)	n	1.53	700	[141]
In_4Se_3	Cu (0.3 wt%)	n	0.97	723	[142]
In_4Se_3	Fe (0.05)	n	0.44	723	[143]
In_4Se_3	In	n	1.13	723	[144]
In_4Se_3	Pb&Sn	n	1.4	773	[145]

to enhancement in electrical conductivity, the effect of alloying scattering on carriers' mobility is also significant. If the effect of doping on increasing carrier concentration does not overcome the decrease of carriers' mobility, electrical conductivity cannot be improved. Therefore, doping should be optimized to a value for which increasing the carrier concentration overcomes the effect of alloying. Figure 12 shows a graph of electrical resistivity versus different iodine contents; resistivity decreases at an optimum doping level, which results in improved electrical conductivity. Doping has been found to have a significant effect on shifting the service temperature at which the peak *ZT* value is achieved. For example, indium doping [85] in *p*-type Bi_2Te_3 showed an enhancement of *ZT* up to 1.4 and shifted the service temperature of Bi_2Te_3 from room temperature range to 500 K. In this study, it was found that doping has a significant effect in broadening the bandgap, hence suppressing the bipolar effect and increasing the Seebeck coefficient. In addition, doping optimized the concentration of intrinsic point defects, which in turn led to a reduction in thermal conductivity. Shifting the maximum *ZT* to a high temperature, 380 K, has been reported when alloying *p*-type Bi_2Te_3 with Sb [86]. Several other studies reported a shift in the service temperature. Liu *et al.* [87] reported a peak *ZT* of 0.8 at 573 K for *n*-type Bi_2Te_2S. Hua *et al.* [88] reported a value of 0.92 at 710 K for *p*-type $Ag_{0.01}Sb_{1.85}In_{0.15}Te_3$. Wang *et al.* [89] reported a peak *ZT* value of 0.86 at 600 K for *n*-type $Bi_2Te_{1.5}Se_{1.5}$. In addition to doping, alloying of elements was found to be an effective method for improving thermoelectric performance but differently from the doping effect. With alloying, the power factor increases while thermal conductivity decreases. The reduction in lattice thermal conductivity is a result of the atomic disorder generated by the alloyed foreign element. The guest material acts as a scattering center for phonons, and the degree of scattering depends on the mass ratio of the alloy constituents [3, 90]. Simultaneously, alloying is an efficient way to improve the power factor by modifying the band structure and creating a path for carrier transport [30]. Alloyed semiconductors with high carrier

concentration are the best bulk thermoelectric materials. The thermoelectric properties of antimony telluride when alloyed with bismuth telluride improve significantly. The power factor and figure of merit of 25% Bi_2Te_3-75% Sb_2Te_3 alloy at room temperature reached 3.1×10^{-3} $Wm^{-1}K^{-2}$ and 0.85, respectively [91]. In another study, the maximum power factor reached 3.81×10^{-3} $Wm^{-1}K^{-2}$ at 300 K and *ZT* reached 0.97 with 80% Sb_2Te_3 [92]. Table 2 summarizes some layered chalcogenide materials doped with various dopants and their *ZT*.

4.2 Nanostructuring

Reducing at least one structural dimension of the thermoelectric materials to the nanoscale range by nanostructuring is a valid approach for improving the figure of merit *ZT*. Nanostructuring can be controlled either by producing nanomaterials such as nanofilms, nanowires, quantum dots, nanoparticles, and superlattices or by decreasing the grain size to the nanoscale range, as in the case of nanobulk materials [3]. Nanostructuring is an efficient way to reduce thermal conductivity and enhance the power factor by generating many interfaces in thermoelectric materials that can block phonon transport. Grain boundaries, especially when the grain size is comparable with the mean free path of phonons, can scatter phonons more efficiently than electrons while acting as a potential barrier for low-energy charge carriers. Filtering of low energy charge carriers has a significant effect on keeping the potential difference through the material and can enhance the Seebeck coefficient [90, 146]. However, in some cases, carrier mobility is affected by the disturbance arising from phonon scattering, leading to a reduction in electrical conductivity [7]. High *ZT* by nanostructure engineering was first proposed theoretically by Hicks and Dresselhause [170]. They published a theoretical model calculating the Seebeck coefficient and thermal conductivity when confining the electron in a two-dimensional quantum well. Their model predicted improvement of *ZT* as a result of enhancing the Seebeck coefficient and reducing thermal conductivity due to phonon scattering at the interfaces. Not long after, Venkatasubramaniam et al. synthesized Bi_2Te_3/Sb_2Te_3 superlattices and reported a high *ZT* value of 2.4 [148]. Several studies have employed nanostructures and successfully produced nanomaterials with a high value of *ZT* due to a reduction in thermal conductivity [3, 149, 150], whereas some other studies reported a significant improvement in the Seebeck coefficient in addition to the reduction of thermal conductivity [24, 149–151]. For example, low thermal conductivity with a total improvement in *ZT* has been achieved in ball-milled *p*-type SnTe as a result of phonon scattering at grain boundaries [82]. A similar improvement due to a significant reduction in thermal conductivity has been achieved in *n*-type $Bi_2Te_{2.7}Se_{0.3}$ ultrathin nanowires. In this study [149], the *ZT* value was increased to 0.95, which is 13% higher than the conventional grain size sample. In contrast, preparing nanobulk Bi_2Te_3 represents a 30% improvement in the power factor compared with the conventional sample, especially at low temperatures (325–425 K) [151]. Wan *et al.* [152] prepared layered metal sulfides (BiS, SnS) with alternative stacking of TiS_2 layer and metal sulfides. In this work, they found several nanoscale stacking fault, including staging disorder for BiS and translational disorder for SnS. The presence of the nanoscale stacking fault results in a reduction of thermal conductivity along the layers demonstrating phonon blocking; the electrical mobility has not deteriorated. However, the amorphous structure with extra boundaries in polycrystals and nanostructured materials has a significant effect on the carriers' transport. Wei *et al.* [79] found that carrier mobility in doped SnSe was lower in the polycrystal sample than in the single-crystal sample. This was attributed to several reasons, including the extra scattering of carriers at grain boundaries and the misorientation of the crystals. Similarly, Dharmaiah and Hong [153] found that the carrier mobility of Sb_2Te_3 nanobulk is decreased due to the scattering of charge carriers at the grain boundaries and the voids. Rarely, it was found that introducing amorphous and fine nanostructure does not affect the electrical conductivity. Xie *et al.* [150] found that electrical conductivity has not decreased in the sintered melt spinning $Bi_{0.52}Sb_{1.48}Te_3$ sample which exhibits a fine and amorphous structure compared with the same zone melted and sintered samples. The authors suggested that this may attributed to the fact that the coherent interfaces between grains can be beneficial to carrier mobility. To a certain extent, they can compensate for the negative effect of amorphous and nanostructure. Table 3 summarizes some layered chalcogenide nanomaterials and their *ZT*.

Table 3: *ZT* of some layered chalcogenides nanostructures.

Nanostructure material	Type	ZT	T, K	Reference
BiSbTe NC bulk	p	1.4	373	[154]
Bulk nanostructured Bi_2Te_3	n	1.1	340	[151]
Nanostructured BiSbTe	p	1.3	373	[155]
Bi_2Te_3 nanoplate	n	0.62	400	[156]
Bi_2Te_3 ultrathin nanowires	n	0.96	380	[149]
Bi_2Te_3 nanoparticles	n	0.62	-	[157]
Nanobulk $Bi_{0.5}Sb_{1.5}Te_3$	p	1	300	[158]
Nanobulk Bi_2Te_3		0.94	398	[159]
Nanobulk $Bi_{0.52}Sb_{1.48}Te_3$	p	1.56	300	[150]
Flower-like Bi_2Te_3 nanosheet	n	1.16	-	[160]
Nanoporous in the bulk Bi_2Te_3	p	1.38	473	[161]
Bulk nanostructured $Bi_{0.4}Sb_{1.6}Te_3$	p	1.12	350	[162]
Bulk nanostructured $Bi_{0.5}Sb_{1.5}Te_3$	p	1.4	300	[163]
Bulk nanostructured $Bi_{0.5}Sb_yTe_{3-y}$	p	0.7	373	[164]
$Bi_{0.4}Sb_{1.6}Te_3$ porous thin film	p	1.8	298	[165]
Bi_2Te_3 nanoparticles	n	0.61	423	[157]
Sb_2Te_3 nanosheet	p	0.58	420	[24]
Sb_2Te_3 nanoplates	p	0.55	400	[153]
Bi_2Se_3 nanoflakes	n	0.096	523	[166]
Bi_2S_3 nanobulk	n	0.5	450	[167]
SnSe nanowires	p	0.156	370	[168]
SnSe thin films	p	0.055	501	[6]
SnSe porous nanosheets	p	0.12	310	[169]

4.3 Nanocompositing

Incorporating a second-phase material, especially a nano additive, into thermoelectric materials to develop a composite is an effective strategy to combine the high electrical conductivity of the base material with the low thermal conductivity of the composite. Introducing a large structured material compared with the nano-additive atom leads to the presence of a high density of interfaces [147]. These interfaces act as barriers to scatter the phonons efficiently and cause decreasing thermal conductivity. In addition, the interfaces scatter and filter low-energy carriers, resulting in an improvement in the Seebeck coefficient without severely affecting electrical conductivity [17, 90, 171–173]. Phonons are scattered more than electrons in nanocomposites because the phonons' mean free path is greater than the carriers' mean free path, leading to stronger scattering of phonons rather than electrons. In some cases, the introduced interfaces lead to a reduction in electrical conductivity, so it is essential to select a proper additive material [174, 175]. Moreover, producing some composites is limited by the high fabrication cost as well as poor scalability and rarity of the element [176]. For several years, a considerable amount of work has been done using different nanoadditives in order to enhance the performance of layered chalcogenide materials. Here, nano-additives are classified into carbon-based and noncarbon materials.

4.3.1 Carbon-Based Layered Materials Composites

Carbon-based materials, including carbon black, carbon nanotubes, graphene, and graphene oxide have been introduced to layered chalcogenide materials. Yeo and Oh [177] found that the dispersion of 0.12% multiwall carbon nanotubes (MWCNT) into *p*-type $(Bi_{0.2}Sb_{0.8})_2Te_3$ matrix improves *ZT* from 1.03 for a pristine sample to 1.41 for the nanocomposite at room temperature. Although the presence of the grain boundaries and MWCNT/$(Bi_{0.2}Sb_{0.8})_2Te_3$ interfaces resulted in extra scattering of the carriers and hence reduced electrical conductivity, the overall improvement is attributed mainly to the reduction of thermal conductivity as a result of strong phonon scattering. Li *et al.* [178] reported a high figure of merit of 1.21 for polycrystalline *p*-type SnSe when incorpo-

Table 4: Comparison between important properties of carbon nanotubes and graphene.

Properties	Carbon nanotubes	Graphene
Electrical conductivity (S m^{-1})	5000	10^6
Thermal conductivity (W/m K)	3000	5000
Fracture strength (GPa)	45	124
Specific surface area (m^2/g)	≈ 100 to 1000	2630 (theoretically)

rated with 2.5 vol% of carbon black. The improvement is attributed mainly to the increase in electrical conductivity resulting in a high power factor. Recently, graphene has gained significant interest for its superior thermoelectric properties. Graphene is the first two-dimensional sheet of hexagonally sp^2 hybridized carbon material arranged into a periodic ring structure. It is the thinnest material available in nature [8, 179–181]. It has high electrical conductivity, and its thermal conductivity is much higher than most materials measured at room temperature [10, 176]. Compared with carbon nanotubes, which exhibit distinctive properties, graphene has higher thermal conductivity and higher electrical conductivity, and it possesses a large surface area that allows interaction with other atoms in the matrix [182]. Table 4 shows a comparison of properties between carbon nanotubes and graphene [181]. The charge transport properties and the carrier mobility enable graphene to be a useful material for thermoelectric devices. Utilizing graphene as an additive for several material matrices has emerged for use in thermoelectric systems in order to develop a high-efficiency composite. A small amount of graphene could play an important role in blocking phonon scattering and reducing the thermal conductivity of the composite. Due to the high electrical mobility of carriers in graphene, it can maintain the electrical conductivity of the composite [3, 183]. Based on a detailed literature review, graphene has not been used with layered chalcogenide materials, except in several studies with bismuth telluride and bismuth selenide [12, 13, 146, 175, 183–194]. However, a common trend observed for all thermoelectric properties is that there is a limited content of graphene for enhancing the properties. Despite the improvement that is achieved in composites with several graphene contents compared with the pure sample [185, 191, 192], most studies have achieved maximum *ZT* with a relatively small amount of graphene. This could be attributed to the aggregation of carriers and scattering at the interfacial boundaries with increasing graphene content [192]. With an optimum amount of graphene, the thermal conductivity of graphene composites has been found to reach a minimum value compared with the pristine samples [12]. Figure 13 shows the thermal conductivity of several composite samples with different graphene contents compared with the pure sample of BiSbTe [191]. The significant reduction of thermal conductivity was attributed to the high density of grain boundaries, defects, and interfaces that could effectively scatter the phonons. The Seebeck coefficient does not show a fixed trend with increasing graphene content. In some studies, the Seebeck coefficient decreased compared with the pure material when adding graphene [12, 146, 190, 192], which is expected as the number of charge carriers accompanied

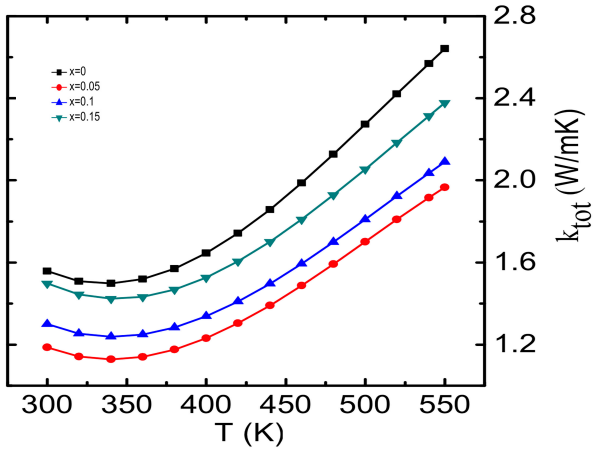

Figure 13: Thermal conductivity as a function of temperature for BiSbTe + x wt% graphene. All composite samples have lower thermal conductivity than the pristine sample. Reproduced from Ref. [191].

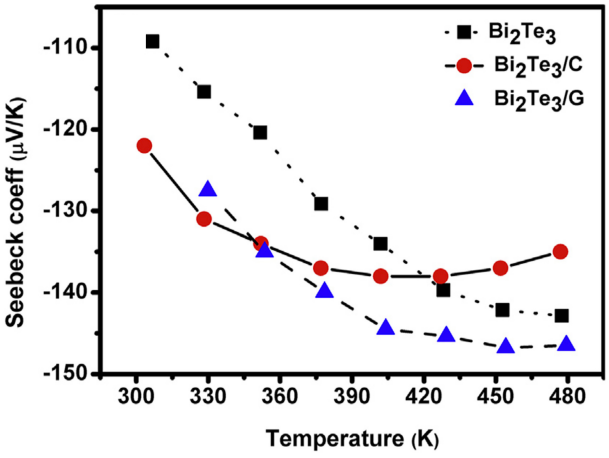

Figure 14: Temperature dependence of the Seebeck coefficient of bulk Bi_2Te_3 and Bi_2Te_3 composite. The addition of graphene leads to an increase in the Seebeck coefficient. Reproduced from Ref. [187].

Table 5: *ZT* of some layered chalcogenides carbon-based composites.

Matrix	Additive type	Optimum loading	Type	ZT	T, K	Ref.
SnSe	Carbon black	2.5 vol%	p	1.21	903	[178]
Bi_2Te_3	Carbon nanotubes	-	n	0.85	473	[195]
Bi_2Te_3	Single-wall carbon nanotube	-	n	ZT enhanced 25-30%		[196]
Bi_2Te_3	GNS	0.2 vol%	n	0.21	475	[190]
Bi_2Te_3	Monolayer graphene	0.05 wt%	n	0.92	402	[187]
Nanowire Bi_2Te_3	GNS	1 wt%	n	0.4	300	[186]
Bi_2Te_3	GQD	0.405	n	0.46	450	[188]
$(Bi_{0.2}Sb_{0.8})_2Te_3$	Multiwall carbon nanotube	x = 0.21 wt%	p	1.47	348	[177]
$Bi_{0.5}Sb_{1.5}Te_3$	Graphite	0.05	p	1.05	320	[197]
$Bi_{0.5}Sb_{1.5}Te_3$	Expanded graphene	0.1 vol%	p	1.13	360	[192]
$Bi_{0.36}Sb_{1.6}4Te_3$	RGO	0.4 vol%	p	1.16	393	[191]
$Bi_{0.4}Sb_{1.6}Te_3$	GNS	0.3 vol% 300K	p	1.29	300	[12]
		0.4 vol% 400 K		x= 0.3 vol% 1.54 x= 0.4 vol %	440	
$Bi_{0.48}Sb_{1.52}Te_3$	GNS	0.05 wt%	p	1.25	320	[175]
$Bi_{0.4}Sb_{1.6}Te_3$	GNS	0.05 wt%	p	1.26	423	[146]
$Bi_{85}Sb_{15}$	Graphene nanoparticles	0.08 wt%	n		173	[11]
$Bi_2Te_{2.4}Se_{0.6}$	Multiwall carbon nanotube	-	n	0.8	425	[198]
$Bi_2(Te_{0.9}Se_{0.1})_3$	Multiwall carbon nanotube	x = 0.015 vol%	n	0.98	423	[199]
$Bi_2Te_{2.7}Se_{0.3}$	Unoxidized graphene nanoplates	0.05 wt%	n	0.8	400	[184]
$Bi_{85}Sb_{15}$	Gr	0.5%	n	0.39	260	[194]

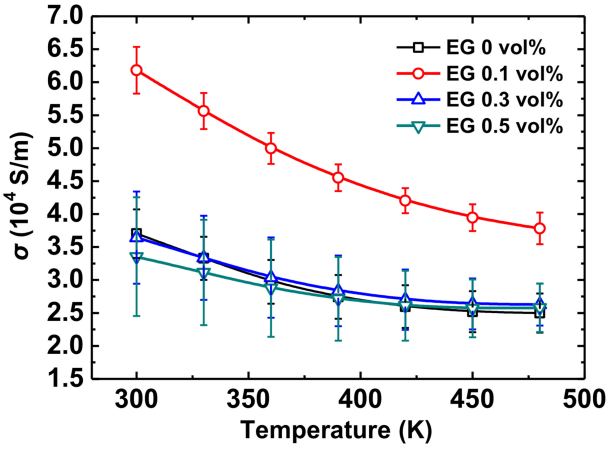

Figure 15: Temperature dependence of electrical conductivity of $Bi_{0.5}Sb_{1.5}Te_3$ – Expanded graphene (EG). Reproduced from Ref. [192].

by the addition of graphene increases [187]. Other studies [184, 187, 190, 191] have shown that Seebeck coefficient followed a reverse trend. Agarwal *et al.* [187] found that the incorporation of monolayer graphene increases the Seebeck coefficient for the composite sample compared with the pure sample as shown in Figure 14. Several studies have shown that electrical conductivity is improved with increasing the graphene content up to a certain optimum limit [146, 175, 192]. This finding was attributed to the presence of the highly conductive graphene [13, 186]. For example, the addition of graphene from x = 0.1 wt% up to 10 wt% except at x = 0.5 wt% was found to increase electrical conductivity for both powder and nanowire *n*-type Bi_2Te_3 composites [186]. At x = 0.5 wt%, the unexpected reduction in electrical conductivity could be attributed to the carrier transport at the interfaces of nanostructured Bi_2Te_3 and graphene, which has different potential energies that affect the composite and result in decreasing carrier concentration. Suh *et al.* [192] found that the incorporation of 0.1% expanded graphene (EG) increases the conductivity in the whole temperature range, as shown in Figure 15. This improvement in electrical conductivity is attributed to the enhancement in both carriers' concentration and mobility indicating an excellent effect of expanded graphene. However, the extra amount of graphene beyond the optimum level leads to a reduction of both carriers' concen-

Table 6: *ZT* of some layered chalcogenides non carbon-based composites.

Matrix	Additive type	Optimum Loading	Type	ZT	T,K	Reference
Bi_2Te_3	Bi semimetal	5 vol%	n	0.4	323	[203]
Bi_2Te_3	Ag	2 vol%	n	0.77	475	[200]
Bi_2Te_3	Ag NW	1.5 vol%	n	0.71	474	[201]
$Bi_{0.5}Sb_{1.5}Te_{0.3}$	Al NP	0.3 vol%	p	1.5	323	[202]
$Bi_{0.4}Sb_{1.6}Te_3$	Cu_7Te_4	5 wt%	p	1.14	444	[204]
$Bi_{0.48}Sb_{1.52}T_{e3}$	WSe_2	-	p	1.27	360	[205]
$Bi_{0.5}Sb_{1.5}Te_3$	SiC	0.1 vol%	p	0.97	323	[174]
$Bi_{0.3}Sb_{1.7}Te_3$	SiC	0.4 vol%	p	1.33	373	[210]
$Bi_{0.5}Sb_{1.5}Te_3$	Cu_3SbSe_4	1 vol%	p	1.6	476	[206]
$Bi_{0.5}Sb_{1.5}Te_3$	Mn	0.2%	p	1.46	320	[162]
$Bi_{0.4}Sb_{1.6}Te_3$	$CuInTe_2$	0.2 wt%	p	1.45	400	[217]
Bi_2Te_3	Al_2O_3	1 vol%	n	0.99	400	[211]
Bi_2Te_3	Bi_2Se_3	10–15%	n	0.7	400	[207]
Bi_2Te_3	Te	-	n	2.27	375	[218]
$Bi_{0.48}Sb_{1.52}Te_3$	PbTe	0.05 atm%	p	-	300	[219]
BiSbTeSe	ZnSb	0.5	p	1.13	410	[220]
$Bi_{0.46}Sb_{1.54}Te_3$	ZnTe	-	p	1.4	400	[221]
TiS_2	Bi	0.05	n	0.03	300	[222]
TiS_2	$PbSnS_3$	0.5 mol%	n	0.44	650	[223]
TiS_2	MoS_2	3 mol %	n	0.29	573	[215]
Bi_2S_3	Bi	-	n	0.36	623	[36]
BiCuSeO	Cu_2Se	20 vol %	p	0.44	823	[214]
BiCuSeO	SiC	8 %	p	1.32	873	[216]
BiCuSeO	$La_{0.8}Sr_{0.2}CoO_3$	20 vol %	p	0.67	873	[224]
SnSe	PbTe	1.5 vol%	p	1.26	880	[208]
SnSe	SnTe	0.5 mol%	p	1.6 ± 0.2	875	[209]
SnSe	SiC	1 wt%	p	0.125	300	[213]
SnSe	MoS_2/G	3.2 wt%	p	0.98	810	[225]
SnSe	Ag2Se	1%	p	0.74	773	[226]
InSe	In_4Se_3	-	n	0.25	600	[63]
InSe/In_4Se_3	$SrTiO_3$	-	n	0.21	600	[63]

tration and mobility due to the aggregation of graphene and scattering at the interfaces. The total improvement in the electrical properties, along with the reduction in the thermal conductivity of the composited samples, leads to a significant improvement in *ZT*. However, the maximum value of *ZT* is limited by the graphene content as well as the temperature where *ZT* is measured. It is worth mentioning that the same sample could have two maximum *ZT* values with different graphene contents at different temperatures. For instance, Li *et al.* [12] found that the sample exhibits maximum *ZT* at 300 K with a graphene content of 0.3 vol%, while it reaches its maximum value with a graphene content of 0.4 vol% at 440 K. Table 5 summarizes different chalcogenide materials with carbon-based composites.

4.3.2 Non–Carbon-Based Layered Material Composites

Besides carbon-based materials, layered materials have been mixed to improve their thermoelectric properties with other noncarbon additives like metals [162, 200–202], semi metals [203], metal alloys [63, 204–209], and ceramics [63, 198, 210–213]. One example is the dispersion of silver nanoparticles in the bismuth telluride matrix [200], which improved *ZT* of the composite approximately three times compared with pristine bismuth telluride. The silver nanoparticles were uniformly dispersed on the grain boundaries and were found to play an effective role in suppressing the grain growth of bismuth telluride as well as creating lots of interfaces and defects within the matrix, forming a hierarchical structure. The hierarchical struc-

ture causes strong scattering of phonons, which reduces the thermal conductivity and enhances the Seebeck coefficient through the carrier filtering effect. Ju and Kim [213] tried to enhance the thermoelectric performance of *p*-type SnSe by introducing SiC into the matrix. They found that the formation of the composite improved the power factor and effectively reduced thermal conductivity. As a result, *ZT* of the composite was larger than the pristine sample. Liu *et al.* [214] introduced copper selenide (Cu_2Se) into *p*-type BiCuSeO. An enhancement in thermoelectric performance was achieved with a 30% increase in *ZT* at 823 K. In this study, It was found that the electrical conductivity of the composite increases due to the high electrical conductivity of Cu_2Se. The Cu_2Se nanoparticles filled the voids among the BiCuSeO grains and acted like electrical contacts among the matrix, which in turn increased electrical conductivity. Accordingly, the Seebeck coefficient while thermal conductivity increased due to the thermal conductivity contribution of charge carriers. However, the 275% increasing in electrical conductivity of the composite overcame the reduction in the Seebeck coefficient and increment of thermal conductivity and enabled the highest ZT value of 0.44. Aside from the overall improvement in *ZT*, it has been found that introducing a second phase material in the matrix can play a significant role in reducing carrier concentration as well as the carriers' mobility. Ye *et al.* [215] prepared the *n*-type $TiS_2 - xMoS_2$ nanocomposite and found that the electrical conductivity decreased compared with the pristine sample in the whole temperature range especially when x increases above 3. They attributed the reduction in electrical conductivity to both a reduction in carriers' concentration and the reduction in carriers' mobility. As MoS_2 sample is *p*-type with hole charge carriers, an electron-hole combination would occur in the composite at the interfaces between MoS_2 and TiS_2 leading to a reduction in carriers' concentration. Moreover, the large difference in bandgap between the TiS_2 and MoS_2 creates a potential barrier that would scatter low energy carriers, hence reducing carriers' mobility. A similar reduction in the electrical conductivity was reported when doping BiCuSeO with SiC. Feng *et al.* [216] suggested that due to the poor electrical conductivity of SiC, the carrier concentration of the composite decreased. Moreover, the presence of SiC nanoparticles reduced the grain size and increased the boundaries where carriers are scattered and filtered, thus suppressing the mobility. Table 6 summarizes some layered material composites with noncarbon additives and their *ZT*.

5 Conclusion and Future Outlook

This paper gave an overview of the properties and structure of layered chalcogenide thermoelectric materials as well as the progress that has been achieved in measuring their thermoelectric performance. It presented a discussion of several strategies that have been used to enhance their thermoelectric properties, including doping and alloying, nanostructuring, and nanocompositing. Doping and alloying have been found to be effective for enhancing the power factor due to electron density modification as well as reducing thermal conductivity due to the scattering of carriers and phonons by the defects induced. Moreover, nanostructuring into several nanoshaped forms improves *ZT*. The scattering of phonons at the interfaces helps to reduce thermal conductivity, while the filtering of low-energy carriers increases the power factor. Similarly, the introduction of second-phase material into the thermoelectric matrix enhances *ZT* by improving the power factor and reducing thermal conductivity. The interfaces created by the additive act as barriers for filtering the low charge carriers and scattering phonons. In this context, we have discussed graphene as a promising nanoadditive material for preparing thermoelectric layered chalcogenide composites. Bismuth telluride has shown a significant improvement in power factor and thermal conductivity when mixed with graphene. Continued research is required in order to prepare low-cost and high-quality materials. As there is still a deficiency in the studies of graphene-layered chalcogenide thermoelectric materials, it is of great interest to study the cases of graphene composites with different chalcogenide materials and report its effects.

Acknowledgement: This work was made possible by NPRP Grant no. NPRP10-0206-170366 from the Qatar National Research Fund (a member of the Qatar Foundation). The statements made herein are solely the responsibility of the authors. The publication of this article was funded by the Qatar National Library.

References

[1] Elsheikh, M. H., M. F. Mohd Sabri, S., B. Mohd Said, M. H. Hassan, M. B. Ali Bashir, and M. Mohamad. A review on thermoelectric renewable energy: Principle parameters that affect their performance. *Renewable & Sustainable Energy Reviews*, Vol. 30, 2014, pp. 337–355.

[2] Han, C., Q. Sun, Z. Li, and S. X. Dou. Thermoelectric enhancement of different kinds of metal chalcogenides. *Advanced Energy Materials*, Vol. 6, No. 15, 2016, id. 1600498.

[3] Gayner, C., and K. K. Kar. Recent advances in thermoelectric materials. *Progress in Materials Science*, Vol. 83, 2016, pp. 330-382.

[4] Ju, H., M. Kim, and J. Kim. A facile fabrication of n-type Bi2Te3 90 nanowire/graphene layer-by-layer hybrid structures and their improved thermoelectric performance. *Chemical Engineering Journal*, Vol. 275, 2015, pp. 102–112.

[5] Han, C., Q. Sun, Z. Li, and S. X. Dou. Thermoelectric enhancement of different kinds of metal chalcogenides. *Advanced Energy Materials*, Vol. 6, No. 15, 2016, id. 1600498.

[6] Burton, M. R., T. Liu, J. McGettrick, S. Mehraban, J. Baker, A. Pockett, et al. Thin film tin selenide (SnSe) thermoelectric generators exhibiting ultralow thermal conductivity. *Advanced Materials*, Vol. 30, No. 31, 2018, id. 1801357.

[7] Han, C., Z. Li, and S. Dou. Recent progress in thermoelectric materials. *Materials Science*, Vol. 59, 2014, pp. 2073–2091.

[8] Xu, Y., Z. Li, and W. Duan, Thermal and thermoelectric properties of graphene. *Small*, Vol. 10, No. 11, 2014, pp. 2182-2199.

[9] Nieto, A., A. Bisht, D. Lahiri, C. Zhang, and A. Agarwal. Graphene reinforced metal and ceramic matrix composites: A review. *International Materials Reviews*, Vol. 62, No. 5, 2017, pp. 241–302.

[10] Kim, H., A. A. Abdala, and C. W. Macosko. Graphene/Polymer Nanocomposites. *Macromolecules*, Vol. 43, No. 16, 2010, pp. 6515–6530.

[11] El-Asfoury, M. S., M. N. A. Nasr, K. Nakamura, and A. Abdel-Moneim. Thermoelectric power factor performance of Bi85Sb15/graphene composite. *Japanese Journal of Applied Physics*, Vol. 55, No. 4, 2016, id. 045802.

[12] Li, C., X. Qin, Y. Li, D. Li, J. Zhang, H. Guo, et al. Simultaneous increase in conductivity and phonon scattering in a graphene nanosheets/(Bi2 Te3)0.2(Sb2 Te3)0.8 thermoelectric nanocomposite. *Journal of Alloys and Compounds*, Vol. 661, 2016, pp. 389–395.

[13] Ju, H., M. Kim, and J. Kim. Preparation of graphene sheets into one-dimensionally nanostructured bulk bismuth telluride for enhancing thermoelectric power factor. *Journal of Materials Science Materials in Electronics*, Vol. 27, No. 4, 2016, pp. 3427–3434.

[14] Tritt, T. M. Thermoelectric phenomena, materials, and applications. *Annual Review of Materials Research*, Vol. 41, No. 1, 2011, pp. 433–448.

[15] Sassi, S., C. Candolfi, J.-B. Vaney, V. Ohorodniichuk, P. Masschelein, A. Dauscher, et al. Assessment of the thermoelectric performance of polycrystalline p-type SnSe. *Applied Physics Letters*, Vol. 104, No. 21, 2014, id. 212105.

[16] Maignan, A., E. Guilmeau, F. Gascoin, Y. Breárd, and V. Hardy. Revisiting some chalcogenides for thermoelectricity. *Science and Technology of Advanced Materials*, Vol. 13, No. 5, 2012, id. 053003.

[17] Culebras, M., C. M. Goḿez, and A. Cantarero. Review on polymers for thermoelectric applications. *Materials (Basel)*, Vol. 7, No. 9, 2014, pp. 6701–6732.

[18] Jood, P., and M. Ohta. Hierarchical architecturing for layered thermoelectric sulfides and chalcogenides. *Materials (Basel)*, Vol. 8, No. 3, 2015, pp. 1124–1149.

[19] Rao, C. N. R., and W. U. Vasudeo. 2D Inorganic Materials Beyond Graphene. World Scientific Publishing Europe Ltd, 2017.

[20] Srivastava, D., G. C. Tewari, and M. Karppinen. Thermoelectric properties of Cu and Cr disordered CuCrX2 (X = S, Se): A first principles study. *Journal of Physics Condensed Matter*, Vol. 26, No. 50, 2014, id. 505501.

[21] Biswas, K., L. D. Zhao, and M. G. Kanatzidis. Tellurium-free thermoelectric: The anisotropic n-type semiconductor Bi2 S3. *Advanced Energy Materials*, Vol. 2, No. 6, 2012, pp. 634–638.

[22] Li, C., J. Zhao, Q. Hu, Z. Liu, Z. Yu, and H. Yan. Crystal structure and transporting properties of Bi2 S3 under high pressure: Experimental and theoretical studies. *Journal of Alloys and Compounds*, Vol. 688, 2016, pp. 329–335.

[23] Kim, J.-H., D. Bilc, S. Loo, J. Short, S. D. Mahanti, T. Hogan, et al. Synthesis and thermoelectric properties of AgBi3S5. Proceedings of Thermoelectric Materials 2003 - Research and Applications, December 1-3, 2003, Boston, MA., United States. *MRS Online Proceedings Library Archive*, Vol. 793, 2003, pp. 201-206.

[24] Dong, G.-H., Y.-J. Zhu, and L.-D. Chen. Microwave-assisted rapid synthesis of Sb2Te3 nanosheets and thermoelectric properties of bulk samples prepared by spark plasma sintering. *Journal of Materials Chemistry*, Vol. 20, No. 10, 2010, pp. 1976–1981.

[25] Li, J., C. Zhang, Y. Yan, J. Yang, B. Shi, Y. Wang, et al. Predicting excellent anisotropic thermoelectric performance of the layered oxychalcogenides BiAgOCh (Ch = S, Se, and Te). *Computational Materials Science*, Vol. 171, 2020, id. 109273.

[26] An, T.-H., Y. S. Lim, H.-S. Choi, W.-S. Seo, C.-H. Park, G.-R. Kim, et al. Point defect-assisted doping mechanism and related thermoelectric transport properties in Pb-doped BiCuOTe. *Journal of Materials Chemistry. A, Materials for Energy and Sustainability*, Vol. 2, No. 46, 2014, pp. 19759–19764.

[27] Barreteau, C., D. Beŕardan, E. Amzallag, L. D. Zhao, and N. Dragoe. Structural and electronic transport properties in Sr-doped BiCuSeO. *Chemistry of Materials*, Vol. 24, No. 16, 2012, pp. 3168–75 3178.

[28] Pei, Y.-L., J. He, J.-F. Li, F. Li, Q. Liu, W. Pan, et al. High thermoelectric performance of oxyselenides: Intrinsically low thermal conductivity of Ca-doped BiCuSeO. *NPG Asia Materials*, Vol. 5, No. 5, 2013, id. e47.

[29] Zhao, L.-D., S. H. Lo, Y. Zhang, H. Sun, G. Tan, C. Uher, et al. Ultralow thermal conductivity and high thermoelectric figure of merit in SnSe crystals. *Nature*, Vol. 508, No. 7496, 2014, pp. 373–377.

[30] Asfandiyar, T. R., Z. Wei, F. H. Li, Y. Sun, C. F. Pan, M. U. Wu, et al. Thermoelectric SnS and SnS-SnSe solid solutions prepared by mechanical alloying and spark plasma sintering: Anisotropic thermoelectric properties. *Scientific Reports*, Vol. 7, No. 1, 2017, id. 43262.

[31] Zhao, L.-D., C. Chang, G. Tan, and M. G. Kanatzidis. SnSe: A remarkable new thermoelectric material. *Energy & Environmental Science*, Vol. 9, No. 10, 2016, pp. 3044–3060.

[32] Wang, C., Y. Chen, J. Jiang, R. Zhang, Y. Niu, T. Zhou, et al. Improved thermoelectric properties of SnS synthesized by chemical precipitation. *RSC Advances*, Vol. 7, No. 27, 2017, pp. 16795–16800.

[33] Wan, C., Y. Wang, N. Wang, and K. Koumoto. Low-thermal-conductivity (MS) 1+x (TiS2)2 (M = Pb, Bi, Sn) misfit layer compounds for bulk thermoelectric materials. *Materials (Basel)*, Vol. 3, No. 4, 2010, pp. 2606–2617.

[34] Jood, P., M. Ohta, H. Nishiate, A. Yamamoto, O. I. Lebedev, D. Berthebaud, et al. Microstructural control and thermoelectric properties of misfit layered sulfides (LaS) 1+ mTS2 (T = Cr, Nb):The natural superlattice systems. *Chemistry of Materials*, Vol. 26, No. 8, 2014, pp. 2684–2692.

[35] Norimatsu, W. *Thermoelectric Materials*. In Modules, Systems, and Applications in Thermoelectrics, D. M. Rowe, Ed. CRC Press,

2012.

[36] Labeǵorre, J., A. Virfeu, A. Bourhim, H. Willeman, T. Barbier, F. Appert, et al. XBi4S7 (X = Mn, Fe): New cost-efficient layered n-type thermoelectric sulfides with ultralow thermal conductivity. *Advanced Functional Materials*, Vol. 29, No. 48, 2019, id. 1904112.

[37] Ge, Z.-H., P. Qin, D. He, X. Chong, D. Feng, Y. H. Ji, et al. Highly enhanced thermoelectric properties of Bi/Bi2 S3 nanocomposites. *ACS Applied Materials & Interfaces*, Vol. 9, No. 5, 2017, pp. 4828–4834.

[38] Chmielowski, R., D. Peŕe, C. Bera, I. Opahle, W. Xie, S. Jacob, et al. Theoretical and experimental investigations of the thermoelectric properties of Bi2S3. *Journal of Applied Physics*, Vol. 117, No. 12, 2015, id. 125103.

[39] Liu, Z., Y. Pei, H. Geng, J. Zhou, X. Meng, W. Cai, W. Liu, and J. Sui. Enhanced thermoelectric performance of Bi2S3 by synergistical action of bromine substitution and copper nanoparticles. *Nano Energy*, Vol. 13, 2015, pp. 554–562.

[40] Lei, H., K. Wang, M. Abeykoon, E. S. Bozin, and C. Petrovic. New layered fluorosulfide SrFBiS2. *Inorganic Chemistry*, Vol. 52, No. 18, 2013, pp. 10685–10689.

[41] Mizuguchi, Y. Material Development and Physical Properties of BiS2-Based Layered Compounds. *Journal of the Physical Society of Japan*, Vol. 88, No. 4, 2019, id. 041001.

[42] Tan, G., S. Hao, J. Zhao, C. Wolverton, and M. G. Kanatzidis. High thermoelectric performance in electron-doped AgBi3S5 with ultralow thermal conductivity. *Journal of the American Chemical Society*, Vol. 139, No. 18, 2017, pp. 6467–6473.

[43] Tewari, G. C., T. S. Tripathi, H. Yamauchi, and M. Karppinen. Thermoelectric properties of layered antiferromagnetic CuCrSe2. *Materials Chemistry and Physics*, Vol. 145, No. 1-2, 2014, pp. 156–161.

[44] Gascoin, F., and A. Maignan. Order–disorder transition in AgCrSe2: A new route to efficient thermoelectrics. *Chemistry of Materials*, Vol. 23, No. 10, 2011, pp. 2510–2513.

[45] Bhattacharya, S., A. Bohra, R. Basu, R. Bhatt, S. Ahmad, K. N. Meshram, et al. High thermoelectric performance of (AgCrSe2) 0.5 (CuCrSe2) 0.5 nano-composites having all-scale natural hierarchical architectures. *Journal of Materials Chemistry. A, Materials for Energy and Sustainability*, Vol. 2, No. 40, 2014, pp. 17122–17129.

[46] Yan, X., B. Poudel, Y. Ma, W. S. Liu, G. Joshi, H. Wang, et al. Experimental studies on anisotropic thermoelectric properties and structures of n-type Bi2Te2.7Se0.3. *Nano Letters*, Vol. 10, No. 9, 2010, pp. 3373–3378.

[47] Liu, X., S. Lee, J. Furdyna, T. Luo, and Y.-H. Zhang, Eds. *Chalcogenide: From 3D to 2D and Beyond*. Woodhead Publishing, 2019.

[48] Carle, M., P. Pierrat, C. Lahalle-Gravier, S. Scherrer, and H. Scherrer. Transport properties of n-type Bi_2 $(Te_{1-x}Se_x)3$ single crystal solid solutions (x≤ 0.05). *Journal of Physics and Chemistry of Solids*, Vol. 56, No. 2, 1995, pp. 201–209.

[49] Xu, P., T. Fu, J. Xin, Y. Liu, P. Ying, X. Zhao, et al. Anisotropic thermoelectric properties of layered compound $SnSe_2$. *Science Bulletin*, Vol. 62, No. 24, 2017, pp. 1663–1668.

[50] Zhao, L.-D., S. H. Lo, Y. Zhang, H. Sun, G. Tan, C. Uher, et al. Ultralow thermal conductivity and high thermoelectric figure of merit in SnSe crystals. *Nature*, Vol. 508, No. 7496, 2014, pp. 373–377.

[51] Chere, E. K., Q. Zhang, K. Dahal, F. Cao, J. Mao, and Z. Ren. Studies on thermoelectric figure of merit of Na-doped p-type polycrystalline SnSe. *Journal of Materials Chemistry. A, Materials for Energy and Sustainability*, Vol. 4, No. 5, 2016, pp. 1848–1854.

[52] Wan, C., Y. Wang, N. Wang, W. Norimatsu, M. Kusunoki, and K. Koumoto. Intercalation: Building a natural superlattice for better thermoelectric performance in layered chalcogenides. *Journal of Electronic Materials*, Vol. 40, No. 5, 2011, pp. 1271–1280.

[53] Sassi, S., C. Candolfi, A. Dauscher, and B. Lenoir. Thermoelectric Properties of the Homologous Compounds Pb5 Bi6 Se14-*x* I*x* (x = 0.0, 0.025, and 0.05). *Journal of Electronic Materials*, Vol. 47, No. 6, 2018, pp. 3198–3202.

[54] Liu, Z., J. Liang, S. Li, S. Peng, and Y. Qian. Synthesis and growth mechanism of Bi2S3 nanoribbons. *Chemistry (Weinheim an der Bergstrasse, Germany)*, Vol. 10, No. 3, 2004, pp. 634–640.

[55] Han, M.-K., Y. Jin, D. H. Lee, and S. J. Kim. Thermoelectric properties of Bi2Te3: CuI and the effect of its doping with Pb atoms. *Materials (Basel)*, Vol. 10, No. 11, 2017, id. 1235.

[56] Gupta, S., N. Vijayan, A. Krishna, K. Thukral, K. K. Maurya, S. Muthiah, et al. Enhancement of thermoelectric figure of merit in Bi_2Se_3 crystals through a necking process. *Journal of Applied Crystallography*, Vol. 48, No. 2, 2015, pp. 533–541.

[57] Ohta, M., S. Satoh, T. Kuzuya, S. Hirai, M. Kunii, and A. Yamamoto. Thermoelectric properties of Ti1+ xS2 prepared by CS2 sulfurization. *Acta Materialia*, Vol. 60, No. 20, 2012, pp. 7232–7240

[58] Guilmeau, E., T. Barbier, A. Maignan, and D. Chateigner. Thermoelectric anisotropy and texture of intercalated TiS2. *Applied Physics Letters*, Vol. 111, No. 13, 2017, id. 133903.

[59] Putri, Y. E., C. Wan, R. Zhang, T. Mori, and K. Koumoto. Thermoelectric performance enhancement of (BiS) 1.2 (TiS2)2 misfit layer sulfide by chromium doping. *Journal of Advanced Ceramics*, Vol.2, No. 1, 2013, pp. 42–48.

[60] Wan, C., *et al.* TiS2-based natural superlattices for bulk thermoelectric materials. In Preprints of 22^{nd} Fall Meeting of The Ceramic Society of Japan.

[61] Miyazaki, Y., H. Ogawa, T. Nakajo, Y. Kikuchii, and K. Hayashi. Crystal structure and thermoelectric properties of misfit-layered sulfides [Ln2 S2] pNbS2 (Ln = Lanthanides). *Journal of Electronic Materials*, Vol. 42, No. 7, 2013, pp. 1335–1339.

[62] Shelimova, L., O. G. Karpinskii, P. P. Konstantinov, E. S. Avilov,M. A. Kretova, G. U. Lubman, et al. Composition and properties of compounds in the PbSe-Bi_2 Se_3 system. *Inorganic Materials*, Vol. 46, No. 2, 2010, pp. 120–126.

[63] Lee, M. H., J.-S. Rhyee, M. Vaseem, Y.-B. Hahn, S.-D. Park, H. Jin Kim, et al. Thermoelectric properties of SrTiO3 nano-particles dispersed indium selenide bulk composites. *Applied Physics Letters*, Vol. 102, No. 22, 2013, id. 223901.

[64] Shi, X., J. Y. Cho, J. R. Salvador, J. Yang, and H. Wang. Thermoelectric properties of polycrystalline In4 Se3 and In4 Te3. *Applied Physics Letters*, Vol. 96, No. 16, 2010, id. 162108.

[65] Tewari, G. C., T. S. Tripathi, P. Kumar, A. K. Rastogi, S. K. Pasha, and G. Gupta. Increase in the thermoelectric eflciency of the disordered phase of layered antiferromagnetic CuCrS2. *Journal of Electronic Materials*, Vol. 40, No. 12, 2011, pp. 2368–2373.

[66] Kaltzoglou, A., P. Vaqueiro, T. Barbier, E. Guilmeau, and A. V. Powell. Ordered-defect sulfides as thermoelectric materials. *Journal of Electronic Materials*, Vol. 43, No. 6, 2014, pp. 2029–2034.

[67] Ruleova, P., C. Drasar, P. Lostak, C.-P. Li, S. Ballikaya, and C. Uher.Thermoelectric properties of Bi2O2Se. *Materials Chemistry and Physics*, Vol. 119, No. 1-2, 2010, pp. 299–302.

[68] Tan, S., L. J. Li, Y. Liu, P. Tong, B. C. Zhao, W. J. Lu, et al. Superconducting and thermoelectric properties of new layered superconductor Bi4 O4 S3. *Physica. C, Superconductivity*, Vol. 483, 2012,

pp. 94–96.
[69] Zhan, B., Y. Liu, X. Tan, J. Lan, Y. Lin, and C.-W. Nan. Enhanced thermoelectric properties of Bi2 O2 Se ceramics by Bi deficiencies. *Journal of the American Ceramic Society*, Vol. 98, No. 8, 2015, pp. 2465–2469.
[70] Liu, Y., L. D. Zhao, Y. Liu, J. Lan, W. Xu, F. Li, et al. Remarkable enhancement in thermoelectric performance of BiCuSeO by Cu deficiencies. *Journal of the American Chemical Society*, Vol. 133, No. 50, 2011, pp. 20112–20115.
[71] Zhu, H., T. Su, H. Li, C. Pu, D. Zhou, P. Zhu, et al. High pressure synthesis, structure and thermoelectric properties of BiCuChO (Ch = S, Se, Te). *Journal of the European Ceramic Society*, Vol. 37, No. 4, 2017, pp. 1541–1546.
[72] Tritt, T. M., and M. Subramanian. Thermoelectric materials, phenomena, and applications: A bird's eye view. *MRS Bulletin*, Vol. 31, No. 3, 2006, pp. 188–198.
[73] Banik, A., S. Roychowdhury, and K. Biswas. The journey of tin chalcogenides towards high-performance thermoelectrics and topological materials. *Chemical Communications*, Vol. 54, No. 50, 2018, pp. 6573–6590.
[74] Das, D., S. Das, P. Singha, K. Malik, A. K. Deb, A. Bhattacharyya, et al. Evolution of phonon anharmonicity in Se-doped Sb2Te3 thermoelectrics. *Physical Review. B*, Vol. 96, No. 6, 2017, id. 064116.
[75] Duong, A. T., V. Q. Nguyen, G. Duvjir, V. T. Duong, S. Kwon, J. Y. Song, et al. Achieving ZT=2.2 with Bi-doped n-type SnSe single crystals. *Nature Communications*, Vol. 7, No. 1, 2016, id. 13713.
[76] Amollo, T. A., G. T. Mola, M. S. K. Kirui, and V. O. Nyamori. Graphene for thermoelectric applications: prospects and challenges. *Critical Reviews in Solid State and Material Sciences*, Vol. 43, No. 2, 2018, pp. 133–157.
[77] Li, D., X. Tan, J. Xu, G. Liu, M. Jin, H. Shao, et al. Enhanced thermoelectric performance in n-type polycrystalline SnSe by PbBr2 doping. *RSC Advances*, Vol. 7, No. 29, 2017, pp. 17906–17912.
[78] Zhou, Y., L. Li, Q. Tan, and J.-F. Li. Thermoelectric properties of Pb-doped bismuth telluride thin films deposited by magnetron sputtering. *Journal of Alloys and Compounds*, Vol. 590, 2014, pp. 362–367.
[79] Wei, T. -R., G. Tan, X. Zhang, C. F. Wu, J. F. Li, V. P. Dravid, et al. Distinct impact of alkali-ion doping on electrical transport properties of thermoelectric p-type polycrystalline SnSe. *Journal of the American Chemical Society*, Vol. 138, No. 28, 2016, pp. 8875– 8882.
[80] Chen, C. -L., H. Wang, Y. -Y. Chen, T. Day, and G. J. Snyder. Thermoelectric properties of p-type polycrystalline SnSe doped with Ag. *Journal of Materials Chemistry. A, Materials for Energy and Sustainability*, Vol. 2, No. 29, 2014, pp. 11171–11176.
[81] Tan, Q., L. -D. Zhao, J. -F. Li, C. -F. Wu, T. -R. Wei, Z. -B. Xing, et al. Thermoelectrics with earth abundant elements: Low thermal con- ductivity and high thermopower in doped SnS. *Journal of Materials Chemistry. A, Materials for Energy and Sustainability*, Vol. 2, No. 41, 2014, pp. 17302–17306.
[82] Zhang, Q., B. Liao, Y. Lan, K. Lukas, W. Liu, K. Esfarjani, et al. High thermoelectric performance by resonant dopant indium in nanostructured SnTe. *Proceedings of the National Academy of Sciences of the United States of America*, Vol. 110, No. 33, 2013, pp. 13261–13266.
[83] Gong, Y., C. Chang, W. Wei, J. Liu, W. Xiong, S. Chai, et al. Extremely low thermal conductivity and enhanced thermoelectric performance of polycrystalline SnSe by Cu doping. *Scripta Materialia*, Vol. 147, 2018, pp. 74–78.
[84] Wu, F., W. Wang, X. Hu, and M. Tang. Thermoelectric properties of I-doped n-type Bi2 Te3-based material prepared by hydrothermal and subsequent hot pressing. *Progress in Natural Science: Materials International*, Vol. 27, No. 2, 2017, pp. 203–207.
[85] Xu, Z., H. Wu, T. Zhu, C. Fu, X. Liu, L. Hu, et al. Attaining high mid-temperature performance in (Bi, Sb)2Te3 thermoelectric materials via synergistic optimization. *NPG Asia Materials*, Vol. 8, No. 9, 2016, pp. e302-e302.
[86] Hu, L. -P., T. -J. Zhu, Y. -G. Wang, H. -H. Xie, Z. -J. Xu, and X. -B. Zhao. Shifting up the optimum figure of merit of p-type bismuth telluride-based thermoelectric materials for power generation by suppressing intrinsic conduction. *NPG Asia Materials*, Vol. 6, No. 2, 2014, pp. e88-e88.
[87] Liu, W., K. C. Lukas, K. McEnaney, S. Lee, Q. Zhang, C. P. Opeil, et al. Studies on the Bi2 Te3 –Bi2 Se3 –Bi2 S3 system for mid-temperature thermoelectric energy conversion. *Energy & Environmental Science*, Vol. 6, No. 2, 2013, pp. 552–560.
[88] Hu, L., T. J. Zhu, X. Q. Yue, X. H. Liu,Y. G. Wang, Z.J. Xu, et al. Enhanced figure of merit in antimony telluride thermoelectric materials by In–Ag co-alloying for mid-temperature power generation. *Acta Materialia*, Vol. 85, 2015, pp. 270–278.
[89] Wang, S., G. Tan, W. Xie, G. Zheng, H. Li, J. Yang, et al. Enhanced thermoelectric properties of Bi2 (Te1-*x* Se*x*) 3-based compounds as n-type legs for low-temperature power generation. *Journal of Materials Chemistry*, Vol. 22, No. 39, 2012, pp. 20943–20951.
[90] Alam, H., and S. Ramakrishna. A review on the enhancement of figure of merit from bulk to nano-thermoelectric materials. *Nano Energy*, Vol. 2, No. 2, 2013, pp. 190–212.
[91] Fan, X., J. Y. Yang, R. G. Chen, H. S. Yun, W. Zhu, S. Q. Bao, et al. Characterization and thermoelectric properties of p-type 25% Bi2Te3–75% Sb2Te3 prepared via mechanical alloying and plasma activated sintering. *Journal of Physics. D, Applied Physics*, Vol. 39, No. 4, 2006, pp. 740–745.
[92] Fan, X., J. Y. Yang, W. Zhu, S. Q. Bao, X. K. Duan, C. J. Xiao, et al. Effect of nominal Sb2Te3 content on thermoelectric properties of p-type (Bi2 Te3)*x* (Sb2 Te3)1-*x* alloys by MA–HP. *Journal of Physics.D, Applied Physics*, Vol. 39, No. 23, 2006, pp. 5069–5073.
[93] Guo, X., J. Qin, X. Lv, L. Deng, X. Jia, H. Ma, et al. Effect of doping indium into a Bi2Te3 matrix on the microstructure and thermoelectric transport properties. *RSC Advances*, Vol. 6, No. 65, 2016, pp. 60736–60740.
[94] Wu, F., H. Song, J. Jia, and X. Hu. Effects of Ce, Y, and Sm dopingon the thermoelectric properties of Bi2Te3 alloy. *Progress in Natural Science: Materials International*, Vol. 23, No. 4, 2013, pp. 408–412.
[95] Han, M. -K., H. Ryu, and S. -J. Kim. Effect of chromium doping on the thermoelectric properties of Bi2Te3: Cr*x*Bi2Te3 and Cr*x*Bi2-*x*Te3. *Journal of Electronic Materials*, Vol. 42, No. 9, 2013, pp. 2758–2763.
[96] Wu, H.-J., and W.-T. Yen. High thermoelectric performance in Cu-doped Bi2Te3 with carrier-type transition. *Acta Materialia*, Vol. 157, 2018, pp. 33–41.
[97] Singh, N. K., J. Pandey, S. Acharya, and A. Soni. Charge carriers modulation and thermoelectric performance of intrinsically p-type Bi2Te3 by Ge doping. *Journal of Alloys and Compounds*, Vol.746, 2018, pp. 350–355.
[98] Tang, Z., L. Hu, T. Zhu, X. Liu, and X. Zhao. High performance n-type bismuth telluride based alloys for mid-temperature power generation. *Journal of Materials Chemistry. C, Materials for Opti-*

cal and Electronic Devices, Vol. 3, No. 40, 2015, pp. 10597–10603.

[99] Yoon, J. S., J. M. Song, J. U. Rahman, S. Lee, W. S. Seo, K. H. Lee, et al. High thermoelectric performance of melt-spun CuxBi0. 5Sb1. 5Te3 by synergetic effect of carrier tuning and phonon engineering. *Acta Materialia*, Vol. 158, 2018, pp. 289–296.

[100] Qin, H., Y. Liu, Z. Zhang, Y. Wang, J. Cao, W. Cai, et al. Improved thermoelectric performance of p-type Bi0. 5Sb1. 5Te3 through Mn doping at elevated temperature. *Materials Today Physics*, Vol. 6, 2018, pp. 31–37.

[101] Mehta, R. J., Y. Zhang, H. Zhu, D. S. Parker, M. Belley, D. J. Singh, et al. Seebeck and figure of merit enhancement in nanostructured antimony telluride by antisite defect suppression through sulfur doping. *Nano Letters*, Vol. 12, No. 9, 2012, pp. 4523–4529.

[102] Zhang, J., X. Y. Qin, H. X. Xin, D. Li, and C. J. Song. Thermoelectric properties of Co-doped TiS2. *Journal of Electronic Materials*, Vol. 40, No. 5, 2011, pp. 980–986.

[103] Guilmeau, E., Y. Breárd, and A. Maignan. Transport and thermoelectric properties in Copper intercalated TiS_2 chalcogenide. *Applied Physics Letters*, Vol. 99, No. 5, 2011, id. 052107.

[104] Ramakrishnan, A., S. Raman, L.-C. Chen, and K.-H. Chen. Enhancement in thermoelectric properties of TiS2 by Sn addition. *Journal of Electronic Materials*, Vol. 47, No. 6, 2018, pp. 3091–3098.

[105] Nunna, R., F. Gascoin, and E. Guilmeau. Tuned thermoelectric properties of TiS1. 5Se0.5 through copper intercalation. *Journal of Alloys and Compounds*, Vol. 634, 2015, pp. 32–36.

[106] Yin, C., Q. Hu, G. Wang, T. Huang, X. Zhou, X. Zhang, et al. Intriguing substitution of conducting layer triggered enhancement of thermoelectric performance in misfit-layered (SnS)1.2(TiS2)2. *Applied Physics Letters*, Vol. 110, No. 4, 2017, id. 043507.

[107] Liu, R., X. Tan, G. Ren, Y. Liu, Z. Zhou, C. Liu, et al. Enhanced thermoelectric performance of Te-doped Bi2 Se3-*x* Te*x* bulks by self-propagating high-temperature synthesis. *Crystals*, Vol. 7, No. 9, 2017, id. 257.

[108] Sun, G., X. Qin, D. Li, J. Zhang, B. Ren, T. Zou, et al. Enhanced thermoelectric performance of n-type Bi2 Se3 doped with Cu. *Journal of Alloys and Compounds*, Vol. 639, 2015, pp. 9–14.

[109] Kulsi, C., K. Kargupta, and D. Banerjee. Effect of nickel doping on thermoelectric properties of Bismuth selenide. *AIP Conference Proceedings*, Vol. 1832, No. 1, 2017, id. 110040.

[110] Zhan, B., Y. Liu, J. Lan, C. Zeng, Y.-H. Lin, and C.-W. Nan. Enhanced thermoelectric performance of Bi2 O2 Se with Ag addition. *Materials (Basel)*, Vol. 8, No. 4, 2015, pp. 1568–1576.

[111] Tan, X., J. Lan, G. Ren, Y. Liu, Y.-H. Lin, and C.-W. Nan. Enhanced thermoelectric performance of n-type Bi2O2Se by Cl-doping at Se site. *Journal of the American Ceramic Society*, Vol. 100, No. 4, 2017, pp. 1494–1501.

[112] Ruleova, P., T. Plechacek, J. Kasparova, M. Vlcek, L. Benes, P. Lostak, et al. Enhanced thermoelectric performance of n-type Bi2O2Se ceramics induced by Ge doping. *Journal of Electronic Materials*, Vol. 47, No. 2, 2018, pp. 1459–1466.

[113] Liu, R., J. Lan, X. Tan, Y. Liu, G. Ren, C. Liu, et al. Carrier concentration optimization for thermoelectric performance enhancement in n-type Bi2 O2 Se. *Journal of the European Ceramic Society*, Vol. 38, No. 7, 2018, pp. 2742–2746.

[114] Zhao, L., D. Berardan, Y. L. Pei, C. Byl, L. Pinsard-Gaudart, and N. Dragoe. Bi1-*x* Sr*x* CuSeO oxyselenides as promising thermoelectric materials. *Applied Physics Letters*, Vol. 97, No. 9, 2010, id. 092118.

[115] Li, J., J. Sui, Y. Pei, C. Barreteau, D. Berardan, N. Dragoe, et al. A high thermoelectric figure of merit ZT> 1 in Ba heavily doped BiCuSeO oxyselenides. *Energy & Environmental Science*, Vol. 5, No. 9, 2012, pp. 8543–8547.

[116] Li, J., J. Sui, C. Barreteau, D. Berardan, N. Dragoe, W. Cai, et al. Thermoelectric properties of Mg doped p-type BiCuSeO oxyselenides. *Journal of Alloys and Compounds*, Vol. 551, 2013, pp. 649–653.

[117] Li, J., J. Sui, Y. Pei, X. Meng, D. Berardan, N. Dragoe, et al. The roles of Na doping in BiCuSeO oxyselenides as a thermoelectric material. *Journal of Materials Chemistry. A, Materials for Energy and Sustainability*, Vol. 2, No. 14, 2014, pp. 4903–4906.

[118] Ren, G., S. Butt, C. Zeng, Y. Liu, B. Zhan, J. Lan, et al. Electrical and thermal transport behavior in Zn-doped BiCuSeO oxyselenides. *Journal of Electronic Materials*, Vol. 44, No. 6, 2015, pp. 1627–1631.

[119] Das, S., R. Chetty, K. Wojciechowski, S. Suwas, and R. C. Mallik. Thermoelectric properties of Sn doped BiCuSeO. *Applied Surface Science*, Vol. 418, 2017, pp. 238–245.

[120] Lan, J. L., Y. C. Liu, B. Zhan, Y. H. Lin, B. Zhang, X. Yuan, et al. Enhanced thermoelectric properties of Pb-doped BiCuSeO ceramics. *Advanced Materials*, Vol. 25, No. 36, 2013, pp. 5086–5090.

[121] Feng, B., X. Jiang, Z. Pan, L. Hu, X. Hu, P. Liu, et al. Preparation, Structure, and enhanced thermoelectric properties of Sm-doped BiCuSeO oxyselenide. *Materials & Design*, Vol. 185, 2020, id. 108263.

[122] An, T.-H., Y. S. Lim, W.-S. Seo, C.-H. Park, M. D. Yoo, C. Park, et al. Effects of K-doping on thermoelectric properties of Bi1-*x* K*x* CuOTe. *Journal of Electronic Materials*, Vol. 46, No. 5, 2017, pp. 2717– 2723.

[123] Brazis, P. W., M. Rocci, D.-Y. Chung, M. G. Kanatzidis, and C. R. Kannewurf. Transport properties of doped CsBi4Te6 thermoelectric materials. *MRS Online Proceedings Library Archive*, Vol. 545, 1998, id. 545. DOI: doi:10.1557/PROC-545-75.

[124] Chung, D.-Y., T. P. Hogan, M. Rocci-Lane, P. Brazis, J. R. Ireland,C. R. Kannewurf, et al. A new thermoelectric material: CsBi4 Te6. *Journal of the American Chemical Society*, Vol. 126, No. 20, 2004, pp. 6414–6428.

[125] Sassi, S., C. Candolfi, C. Gendarme, A. Dauscher, and B. Lenoir. Synthesis and transport properties of the Te-substituted homologous compounds Pb5 Bi6 Se14-*x* Te*x* ($0 \leq x \leq 1.0$). *Dalton Transactions (Cambridge, England)*, Vol. 47, No. 13, 2018, pp. 4714–4721.

[126] Ge, Z. H., D. Song, X. Chong, F. Zheng, L. Jin, X. Qian, et al. Boosting the thermoelectric performance of (Na,K)-codoped polycrystalline SnSe by synergistic tailoring of the band structure and atomic-scale defect phonon scattering. *Journal of the American Chemical Society*, Vol. 139, No. 28, 2017, pp. 9714–9720.

[127] Li, J. C., D. Li, X. Y. Qin, and J. Zhang. Enhanced thermoelectric performance of p-type SnSe doped with Zn. *Scripta Materialia*, Vol. 126, 2017, pp. 6–10.

[128] Gao, J. L., H. Zhu, T. Mao, L. Zhang, J. Di, and G. Xu. The effect of Sm doping on the transport and thermoelectric properties of SnSe. *Materials Research Bulletin*, Vol. 93, 2017, pp. 366–372.

[129] Zhang, Q., E. K. Chere, J. Sun, F. Cao, K. Dahal, S. Chen, et al. Studies on Thermoelectric Properties of n-type Polycrystalline SnSe1-*x* Sx by Iodine Doping. *Advanced Energy Materials*, Vol. 5, No. 12, 2015, id. 1500360.

[130] Wang, X., J. Xu, G. Liu, Y. Fu, Z. Liu, X. Tan, et al. Optimization of thermoelectric properties in n-type SnSe doped with $BiCl_3$. *Applied Physics Letters*, Vol. 108, No. 8, 2016, id. 083902.

[131] Li, F., W. Wang, Z. -H. Ge, Z. Zheng, J. Luo, P. Fan, and B. Li. Enhanced thermoelectric properties of polycrystalline SnSe via LaCl3 doping. *Materials (Basel)*, Vol. 11, No. 2, 2018, id. 203.

[132] Li, S., Y. Wang, C. Chen, X. Li, W. Xue, X. Wang, Z. Zhang, et al. Heavy doping by bromine to improve the thermoelectric properties of n-type polycrystalline SnSe. *Advancement of Science*, Vol. 5, No. 9, 2018, id. 1800598.

[133] Fu, Y., J. Xu, G.-Q. Liu, X. Tan, Z. Liu, X. Wang, et al. Study on thermoelectric properties of polycrystalline SnSe by Ge doping. *Journal of Electronic Materials*, Vol. 46, No. 5, 2017, pp. 3182–3186.

[134] Wubieneh, T. A., C.-L. Chen, P. C. Wei, S.-Y. Chen, and Y.-Y. Chen. The effects of Ge doping on the thermoelectric performance of p-type polycrystalline SnSe. *RSC Advances*, Vol. 6, No. 115, 2016, pp. 114825–114829.

[135] Singh, N. K., S. Bathula, B. Gahtori, K. Tyagi, D. Haranath, and A. Dhar. The effect of doping on thermoelectric performance of p-type SnSe: Promising thermoelectric material. *Journal of Alloys and Compounds*, Vol. 668, 2016, pp. 152–158.

[136] Bhat, D. K., and U. S. Shenoy. Enhanced thermoelectric performance of bulk tin telluride: Synergistic effect of calcium and indium co-doping. *Materials Today Physics*, Vol. 4, 2018, pp. 12–18.

[137] Zhou, B., S. Li, W. Li, J. Li, X. Zhang, S. Lin, et al. Thermoelectric Properties of SnS with Na-doping. *ACS Applied Materials & Interfaces*, Vol. 9, No. 39, 2017, pp. 34033–34041.

[138] Wu, H., X. Lu, G. Wang, K. Peng, H. Chi, B. Zhang, et al. Sodium-doped tin sulfide single crystal: A nontoxic earth-abundant material with high thermoelectric performance. *Advanced Energy Materials*, Vol. 8, No. 20, 2018, id. 1800087.

[139] Fu, H., P. Ying, J. Cui, Y. Yan, and X. Zhang. Thermoelectric properties of an Al-doped In-Sn-Te-based alloy. *Journal of Electronic Materials*, Vol. 40, No. 5, 2011, pp. 937–941.

[140] Zhai, Y., Q. Zhang, J. Jiang, T. Zhang, Y. Xiao, S. Yang, et al. Thermoelectric properties of In1.3-*x*Sn*x*Se prepared by spark plasma sintering method. *Journal of Alloys and Compounds*, Vol. 553, 2013, pp. 270–272.

[141] Rhyee, J. S., K. Ahn, K. H. Lee, H. S. Ji, and J. H. Shim. Enhancement of the thermoelectric figure-of-merit in a wide temperature range in In(4) Se(3-x) Cl(0.03) bulk crystals. *Advanced Materials*, Vol. 23, No. 19, 2011, pp. 2191–2194.

[142] Li, G., J. Yang, Y. Luo, Y. Xiao, L. Fu, M. Liu, et al. Improvement of thermoelectric properties of In4Se3 bulk materials with Cu nanoinclusions. *Journal of the American Ceramic Society*, Vol. 96, No. 9, 2013, pp. 2703–2705.

[143] Li, G., J. Yang, Y. Xiao, L. Fu, J. Peng, Y. Deng, et al. Effect of Fe substitution on thermoelectric properties of Fe*x* In4-*x* Se3 compounds. *Journal of Electronic Materials*, Vol. 42, No. 4, 2013, pp. 675–678.

[144] Rawat, P. K., H. Park, J. Hwang, and W. Kim. Low Thermal conductivity and high thermoelectric performance in In4Se3-*x* with phase-separated indium inclusions. *Journal of Electronic Materials*, Vol. 46, No. 3, 2017, pp. 1444–1450.

[145] Yin, X., J. Y. Liu, L. Chen, and L. M. Wu. High thermoelectric performance of In4 Se3-based materials and the influencing factors. *Accounts of Chemical Research*, Vol. 51, No. 2, 2018, pp. 240–247.

[146] Zhang, Y., H. Ma, B. Sun, B. Liu, H. Liu, L. Kong, et al. Thermoelectric performance of graphene com- posited BiSbTe bulks by high pressure synthesis. *Alloys and Compounds*, Vol. 715, 2017, pp. 344-348.

[147] Minnich, A., M. S. Dresselhaus, Z. F. Ren, and G. Chen. Bulk nanostructured thermoelectric materials: Current research and future prospects. *Energy & Environmental Science*, Vol. 2, No. 5, 2009, pp. 466–479.

[148] Venkatasubramanian, R., E. Siivola, T. Colpitts, and B. O'Quinn. Thin-film thermoelectric devices with high room-temperature figures of merit. *Nature*, Vol. 413, No. 6856, 2001, pp. 597–602.

[149] Zhang, G., B. Kirk, L. A. Jauregui, H. Yang, X. Xu, Y. P. Chen, et al. Rational synthesis of ultrathin n-type Bi2Te3 nanowires with enhanced thermoelectric properties. *Nano Letters*, Vol. 12, No. 1, 2012, pp. 56–60.

[150] Xie, W., X. Tang, Y. Yan, Q. Zhang, and T. M. Tritt. High thermoelectric performance BiSbTe alloy with unique low-dimensional structure. *Journal of Applied Physics*, Vol. 105, No. 11, 2009, id. 113713.

[151] Saleemi, M., M. S. Toprak, S. Li, M. Johnsson, and M. Muhammed. Synthesis, processing, and thermoelectric properties of bulk nanostructured bismuth telluride (Bi2Te3). *Journalof Materials Chemistry*, Vol. 22, No. 2, 2012, pp. 725–730.

[152] Wan, C., Y. Wang, W. Norimatsu, M. Kusunoki, and K. Koumoto. Nanoscale stacking faults induced low thermal conductivity in thermoelectric layered metal sulfides. *Applied Physics Letters*, Vol. 100, No. 10, 2012, id. 101913.

[153] Dharmaiah, P., and S. J. Hong. Hydrothermal method for the synthesis of Sb2Te3, and Bi0.5Sb1.5Te3 nanoplates and their thermoelectric properties. *International Journal of Applied Ceramic Technology*, Vol. 15, No. 1, 2018, pp. 132–139.

[154] Poudel, B., Q. Hao, Y. Ma, Y. Lan, A. Minnich, B. Yu, et al. High-thermoelectric performance of nanostructured bismuth antimony telluride bulk alloys. *Science*, Vol. 320, No. 5876, 2008, pp. 634–638.

[155] Ma, Y., Q. Hao, B. Poudel, Y. Lan, B. Yu, D. Wang, et al. Enhanced thermoelectric figure-of-merit in p-type nanostructured bismuth antimony tellurium alloys made from elemental chunks. *Nano Letters*, Vol. 8, No. 8, 2008, pp. 2580–2584.

[156] Son, J. S., M. K. Choi, M. K. Han, K. Park, J. Y. Kim, S. J. Lim, et al. n-Type nanostructured thermoelectric materials prepared from chemically synthesized ultrathin Bi2Te3 nanoplates. *Nano Letters*, Vol. 12, No. 2, 2012, pp. 640–647.

[157] Kim, C., D. H. Kim, Y. S. Han, J. S. Chung, S. H. Park, and H. Kim. Fabrication of bismuth telluride nanoparticles using a chemical synthetic process and their thermoelectric evaluations. *Powder Technology*, Vol. 214, No. 3, 2011, pp. 463–468.

[158] Lee, G., and G. Ha. Synthesis of Bi0.5Sb1.5Te3 thermoelectric powder using an oxide-reduction process. *Journal of Electronic Materials*, Vol. 43, No. 6, 2014, pp. 1697–1702.

[159] Yu, F., J. Zhang, D. Yu, J. He, Z. Liu, B. Xu, et al. Enhanced thermoelectric figure of merit in nanocrystalline Bi2Te3 bulk. *Journal of Applied Physics*, Vol. 105, No. 9, 2009, id. 094303.

[160] Wu, F., H. Song, F. Gao, W. Shi, J. Jia, and X. Hu. Effects of different morphologies of Bi2Te3 nanopowders on thermoelectric properties. *Journal of Electronic Materials*, Vol. 42, No. 6, 2013,pp. 1140–1145.

[161] Zhang, Y., G. Y. Xu, F. Han, Z. Wang, and C. C. Ge. Preparation and thermoelectric properties of nanoporous Bi2 Te3-based alloys. *Journal of Electronic Materials*, Vol. 39, No. 9, 2010, pp. 1741–

1745.

[162] Hwang, S., S. -I. Kim, K. Ahn, J. W. Roh, D.-J. Yang, S.-M. Lee, et al. Enhancing the thermoelectric properties of p-type bulk Bi-Sb-Te nanocomposites via solution-based metal nanoparticle decoration. *Journal of Electronic Materials*, Vol. 42, No. 7, 2013, pp. 1411–1416.

[163] Bulat, L., V. T. Bublik, I. A. Drabkin, V. V. Karataev, V. B. Osvenskii, Y. N. Parkhomenko, et al. Bulk nanostructured polycrystalline p-Bi-Sb-Te thermoelectrics obtained by mechanical activation method with hot pressing. *Journal of Electronic Materials*, Vol. 39, No. 9, 2010, pp. 1650–1653.

[164] Kim, C., D. H. Kim, J. S. Kim, Y. S. Han, J. S. Chung, and H. Kim. A study of the synthesis of bismuth tellurium selenide nanocompounds and procedures for improving their thermoelectric performance. *Journal of Alloys and Compounds*, Vol. 509, No. 39, 2011, pp. 9472–9478.

[165] Kashiwagi, M., S. Hirata, K. Harada, Y. Zheng, K. Miyazaki, M. Yahiro, et al. Enhanced figure of merit of a porous thin film of bismuth antimony telluride. *Applied Physics Letters*, Vol. 98, No. 2, 2011, id. 023114.

[166] Kadel, K., L. Kumari, W. Z. Li, J. Y. Huang, and P. P. Provencio. Synthesis and thermoelectric properties of Bi2Se3 nanostructures. *Nanoscale Research Letters*, Vol. 6, No. 1, 2011, id. 57.

[167] Liu, W., C. F. Guo, M. Yao, Y. Lan, H. Zhang, Q. Zhang, et al. Bi2S3 nanonetwork as precursor for improved thermoelectric performance. *Nano Energy*, Vol. 4, 2014, pp. 113–122.

[168] Hernandez, J. A., A. Ruiz, L. F. Fonseca, M. T. Pettes, M. Jose-Yacaman, and A. Benitez. Thermoelectric properties of SnSe nanowires with different diameters. *Scientific Reports*, Vol. 8, No. 1, 2018, id. 11966.

[169] Ju, H., K. Kim, D. Park, and J. Kim. Fabrication of porous SnSeS nanosheets with controlled porosity and their enhanced thermoelectric performance. *Chemical Engineering Journal*, Vol. 335, 2018, pp. 560–566.

[170] Aksamija, Z. Lattice thermal transport in Si-based nanocomposites for thermoelectric applications. *Electronic Materials*, Vol. 44, No. 6, 2015, pp. 1644–1650.

[171] Feng, B., J. Xie, G. Cao, T. Zhu, and X. Zhao. Enhanced thermoelectric properties of p-type CoSb3 /graphene nanocomposite. *Journal of Materials Chemistry. A, Materials for Energy and Sustainability*, Vol. 1, No. 42, 2013, pp. 13111–13119.

[172] Chen, H., C. Yang, H. Liu, G. Zhang, D. Wan, and F. Huang. Thermoelectric properties of CuInTe2-graphene composites. *Royal Society of Chemistry*, Vol. 15, 2013, pp. 6648– 6651.

[173] Zong, P.-a., R. Hanus, M. Dylla, Y. Tang, J. Liao, Q. Zhang, et al. Skutterudite with graphene-modified grain- boundary complexion enhances zT enabling high-efficiency thermoelectric device. *Energy & Environmental Science*, Vol. 10, No. 1, 2017, pp.183-191.

[174] Liu, D.-W., J.-F. Li, C. Chen, and B.-P. Zhang. Effects of SiC nanodispersion on the thermoelectric properties of p-type and n-type Bi2 Te_3-based alloys. *Journal of Electronic Materials*, Vol. 40, No. 5, 2011, pp. 992–998.

[175] Xie, D., J. Xu, G. Liu, Z. Liu, H. Shao, X. Tan, et al. Synergistic optimization of thermoelectric performance in p-type Bi0.48Sb1.52Te3/graphene composite. *Energies*, Vol. 9, No. 4, 2016, id. 236.

[176] Twombly, C. A study of thermoelectric properties of graphene materials. Master Thesis. Trustees of the Colorado School of Mines, Mines Theses & Dissertations, 2015.

[177] Yeo, Y., and T. Oh. Thermoelectric properties of p-type (Bi, $Sb)_2Te_3$ nanocomposites dispersed with multiwall carbon nanotubes. *Materials Research Bulletin*, Vol. 58, 2014, pp. 54–58.

[178] Li, J., D. Li, W. Xu, X. Y. Qin, Y. Y. Li, and J. Zhang. Enhanced thermoelectric performance of SnSe based composites with carbon black nanoinclusions. *Applied Physics Letters*, Vol. 109, No. 17, 2016, id. 173902.

[179] Allen, M. J., V. C. Tung, and R. B. Kaner, Honeycomb carbon: A review of graphene. *American Chemical Society*, Vol. 110, 2010, pp. 132-145.

[180] Liu, F., M.-H. Jang, H. D. Ha, J. -H. Kim, Y. -H. Cho, and T. S. Seo. Facile Synthetic Method for Pristine Graphene Quantum Dots and Graphene Oxide Quantum Dots: Origin of Blue and Green Luminescence. *Advanced Materials*, Vol. 25, 2013, pp. 3657-3662.

[181] Dey, A., O. P. Bajpai, A. K. Sikder, S. Chattopadhyay, and M. A. Shafeeuulla Khan. Recent advances in CNT/graphene based thermoelectric polymer nanocomposite: A proficient move towards waste energy harvesting. *Renewable & Sustainable Energy Reviews*, Vol. 53, 2016, pp. 653–671.

[182] Sruti, A. N., and K. Jagannadham. Electrical Conductivity of Graphene Composites with In and In-Ga Alloy. *Electronic Materials*, Vol. 39, No. 8, 2010, pp. 1268–1276.

[183] Li, A. H., M. Shahbazi, S. H. Zhou, G. X. Wang, C. Zhang, P. Jood, et al. Electronic structure and thermoelectric properties of Bi2Te3 crystals and graphene-doped Bi2 Te3. *Thin Solid Films*, Vol. 518, No. 24, 2010, pp. E57–E60.

[184] Kim, J., E. S. Lee, J. -Y. Kim, S. -M. Choi, K. H. Lee, and W. -S. Seo. Thermoelectric properties of unoxidized graphene/Bi2Te2.7Se0.3 composites synthesized by exfoliation/re-assembly method. physical status solidi (RRL). *Rapid Research Letters*, Vol. 8, No. 4, 2014, pp. 357–361.

[185] Liang, B. B., Y. Li, L. L. Xu, L. J. Wang, W. Jiang. Synthesis of Bi0.5Sb1.5Te3/graphene composite powders. *Materials Science Forum*, Vol. 743-744, 2013, pp. 83–87.

[186] Ju, H., and J. Kim. Preparation and structure dependent thermoelectric properties of nanostructured bulk bismuth telluride with graphene. *Journal of Alloys and Compounds*, Vol. 664, 2016, pp. 639-647.

[187] Agarwal, K., V. Kaushik, D. Varandania, A. Dhar, and B. R. Mehta. Nanoscale thermoelectric properties of Bi2Te3 - graphene nanocomposites: Conducting atomic force, scanning thermal and kelvin probe microscopy studies. *Alloys and Compounds*, Vol. 681, 2016, pp. 394-401.

[188] Li, S., T. Fan, X. Liu, F. Liu, H. Meng, Y. Liu, et al. Graphene quantum dots embedded in Bi2Te3 nanosheets to enhance thermoelectric performance. *ACS Applied Materials & Interfaces*, Vol. 9, No. 4, 2017, pp. 3677–3685.

[189] Facile synthesis and temperature dependent thermoelectric properties of Bi2 Te3 nanowire/graphene layered structures. 2015, pp. 57-57.

[190] Liang, B. B., Z. Song, M. Wang, L. Wang, and W. Jiang. Fabrication and Thermoelectric Properties of Graphene/Bi2 Te3 Composite Materials. *Journal of Nanomaterials*, Vol. 2013, 2013, pp. 1–5.

[191] Shin, W. H., K. Ahn, M. Jeong, J. S. Yoon, J. M. Song, S. Lee, et al. Enhanced thermoelectric performance of reduced graphene oxide incorporated bismuth-antimony-telluride by lattice thermal conductivity reduction. *Journal of Alloys and Compounds*, Vol. 718, 2017, pp. 342–348.

[192] Suh, D., S. Lee, H. Mun, S. -H. Park, K. H. Lee, S. Wng Kim, et al. Enhanced thermoelectric performance of Bi0.5Sb1.5Te3-

expanded graphene composites by simultaneous modulation of electronic and thermal carrier transport. *Nano Energy*, Vol. 13, 2015, pp. 67–76.

[193] Ju, H., and J. Kim. The effect of temperature on thermoelectric properties of n-type Bi2Te3 nanowire/graphene layer-by-layer hybrid composites. *Dalton Transactions (Cambridge, England)*,Vol. 44, No. 26, 2015, pp. 11755–11762.

[194] El-Asfoury, M. S., M. N. A. Nasr, K. Nakamura, and A. Abdel-Moneim. Enhanced thermoelectric performance of Bi85 Sb15 - graphene composite by modulation carrier transport and density of state effective mass. *Journal of Alloys and Compounds*, Vol. 745, 2018, pp. 331–340.

[195] Kim, K. T., S. Y. Choi, E. H. Shin, K. S. Moon, H. Y. Koo, G.-G. Lee, et al. The influence of CNTs on the thermoelectric properties of a CNT/Bi2Te3 composite. *Carbon*, Vol. 52, 2013, pp. 541–549.

[196] Zhang, Y., X. L. Wang, W. K. Yeoh, R. K. Zheng, and C. Zhang. Electrical and thermoelectric properties of single-wall carbon nanotube doped Bi2 Te3. *Applied Physics Letters*, Vol. 101, No. 3, 2012, id. 031909.

[197] Hu, W., H. Zhou, X. Mu, D. He, P. Ji, W. Hou, et al. Preparation and thermoelectric properties of graphite/Bi0.5Sb1.5Te3 composites. *Journal of Electronic Materials*, Vol. 47, No. 6, 2018, pp. 3344–3349.

[198] Lognone; Q., and F. Gascoin. On the effect of carbon nanotubes on the thermoelectric properties of n-Bi2Te2.4Se0.6 made by mechanical alloying. *Journal of Alloys and Compounds*, Vol. 635, 2015, pp. 107–111.

[199] Park, D. -H., M. -Y. Kim, and T. -S. Oh. Thermoelectric energy-conversion characteristics of n-type Bi2(Te, Se)3 nanocomposites processed with carbon nanotube dispersion. *Current Applied Physics*, Vol. 11, No. 4, 2011, pp. S41–S45.

[200] Zhang, Q., X. Ai, L. Wang, Y. Chang, W. Luo, W. Jiang, et al. Improved thermoelectric performance of silver nanoparticles-dispersed Bi2Te3 composites deriving from hierarchical two-phased heterostructure. *Advanced Functional Materials*, Vol. 25, No. 6, 2015, pp. 966–976.

[201] Zhang, Q., X. Ai, W. Wang, L. Wang, and W. Jiang. Preparation of 1-D/3-D structured AgNWs/Bi2Te3 nanocomposites with enhanced thermoelectric properties. *Acta Materialia*, Vol. 73, 2014, pp. 37–47.

[202] Kim, K. T., and G. H. Ha. Fabrication and enhanced thermoelectric properties of alumina nanoparticle-dispersed Bi0.5Sb1.5Te3 matrix composites. *Journal of Nanomaterials*, Vol. 2013, 2013, id. 8.

[203] Sumithra, S., N. J. Takas, D. K. Misra, W. M. Nolting, P. F. P. Poudeu, and K. L. Stokes. Enhancement in thermoelectric figure of merit in nanostructured Bi2 Te3 with semimetal nanoinclusions. *Advanced Energy Materials*, Vol. 1, No. 6, 2011, pp. 1141–1147.

[204] Tan, L. P., T. Sun, S. Fan, L. Y. Ng, A. Suwardi, Q. Yan, et al. Facile synthesis of Cu_7Te_4 nanorods and the enhanced thermoelectric properties of Cu7Te4–Bi0.4Sb1.6Te3 nanocomposites. *Nano Energy*, Vol. 2, No. 1, 2013, pp. 4–11.

[205] Xiao, Y., G. Chen, H. Qin, M. Wu, Z. Xiao, J. Jiang, et al. Enhanced thermoelectric figure of merit in p-type Bi 0.48 Sb 1.52 Te 3 alloy with WSe2 addition. *Journal of Materials Chemistry. A, Materials for Energy and Sustainability*, Vol. 2, No. 22, 2014, pp. 8512–8516.

[206] Li, Y., D. Li, X. Qin, X. Yang, Y. Liu, J. Zhang, et al. Enhanced thermoelectric performance through carrier scattering at hetero-junction potentials in BiSbTe based composites with Cu3SbSe4 nanoinclusions. *Journal of Materials Chemistry. C, Materials for Optical and Electronic Devices*, Vol. 3, No. 27, 2015, pp. 7045–7052.

[207] Min, Y., J. W. Roh, H. Yang, M. Park, S. I. Kim, S. Hwang, et al. Surfactant-free scalable synthesis of Bi2Te3 and Bi2Se3 nanoflakes and enhanced thermoelectric properties of their nanocomposites. *Advanced Materials*, Vol. 25, No. 10, 2013, pp. 1425–1429.

[208] Li, D., J. C. Li, X. Y. Qin, J. Zhang, H. X. Xin, C. J. Song, et al. Enhanced thermoelectric performance in SnSe based composites with PbTe nanoinclusions. *Energy*, Vol. 116, 2016, pp. 861–866.

[209] Guo, H., H. Xin, X. Qin, J. Zhang, D. Li, Y. Li, et al. Enhanced thermoelectric performance of highly oriented polycrystalline SnSe based composites incorporated with SnTe nanoinclusions. *Journal of Alloys and Compounds*, Vol. 689, 2016, pp. 87–93.

[210] Li, J., Q. Tan, J.-F. Li, D.-W. Liu, F. Li, Z.-Y. Li, et al. BiSbTe-Based Nanocomposites with High ZT: The Effect of SiC Nanodispersion on Thermoelectric Properties. *Advanced Functional Materials*, Vol. 23, No. 35, 2013, pp. 4317–4323.

[211] Li, F., X. Huang, Z. Sun, J. Ding, J. Jiang, W. Jiang, et al. Enhanced thermoelectric properties of n-type Bi2 Te3 -based nanocomposite fabricated by spark plasma sintering. *Journal of Alloys and Compounds*, Vol. 509, No. 14, 2011, pp. 4769–4773.

[212] Wang, Y., J. Wen, Z. Fan, N. Bao, R. Huang, R. Tu, et al. Energy-filtering-induced high power factor in PbS-nanoparticles- embedded TiS2. *AIP Advances*, Vol. 5, No. 4, 2015, id. 047126.

[213] Ju, H., and J. Kim. Effect of SiC ceramics on thermoelectric properties of SiC/SnSe composites for solid-state thermoelectric applications. *Ceramics International*, Vol. 42, No. 8, 2016, pp. 9550–9556.

[214] Liu, Y., Y. Zhou, J. Lan, C. Zeng, Y. Zheng, B. Zhan, et al. Enhanced thermoelectric performance of BiCuSeO composites with nanoinclusion of copper selenides. *Journal of Alloys and Compounds*, Vol. 662, 2016, pp. 320–324.

[215] Ye, Y., Y. Wang, Y. W. Shen, Y. Wang, L. Pan, R. Tu, et al. Enhanced thermoelectric performance of xMoS2 –TiS2 nanocomposites. *Journal of Alloys and Compounds*, Vol. 666, 2016, pp. 346–351.

[216] Feng, B., G. Li, X. Hu, P. Liu, R. Li, Y. Zhang, et al. Improvement of thermoelectric and mechanical properties of BiCuSeO-based materials by SiC nanodispersion. *Journal of Alloys and Compounds*, Vol. 818, 2020, id. 152899.

[217] Wang, Y., L. L. Huang, D. Li, J. Zhang, and X. Y. Qin. Enhanced thermoelectric performance of Bi0.4Sb1.6Te3 based composites with CuInTe2 inclusions. *Journal of Alloys and Compounds*, Vol. 758, 2018, pp. 72–77.

[218] Choi, H., K. Jeong, J. Chae, H. Park, J. Baeck, T. H. Kim, et al. Enhancement in thermoelectric properties of Te-embedded Bi2Te3 by preferential phonon scattering in heterostructure interface. *Nano Energy*, Vol. 47, 2018, pp. 374–384.

[219] Liang, S., J. Xu, H. Wang, X. Tan, G.-Q. Liu, H. Shao, et al. Investigation on structure and thermoelectric properties in p-type Bi0.48Sb1.52Te3 via PbTe incorporating. *Journal of Materials Science Materials in Electronics*, Vol. 29, No. 9, 2018, pp. 7701–7706.

[220] Zhang, T., J. Jiang, Y. Xiao, Y. Zhai, S. Yang, and G. Xu. Enhanced thermoelectric figure of merit in p-type BiSbTeSe alloy with ZnSb addition. *Journal of Materials Chemistry. A, Materials for Energy and Sustainability*, Vol. 1, No. 3, 2013, pp. 966–969.

[221] Deng, R., X. Su, S. Hao, Z. Zheng, M. Zhang, H. Xie, et al. High thermoelectric performance in Bi0.46Sb1.54Te3 nanostructured with ZnTe. *Energy & Environmental Science*, Vol. 11, No. 6, 2018, pp. 1520–1535.

[222] Li, D., X. Y. Qin, J. Zhang, L. Wang, and H. J. Li. Enhanced thermoelectric properties of bismuth intercalated compounds Bi*x* TiS2 . *Solid State Communications*, Vol. 135, No. 4, 2005, pp. 237–240.

[223] Zhang, J., Y. Ye, C. Li, J. Yang, H. Zhao, X. Xu, *et al.* Thermoelectric properties of TiS2-xPbSnS3 nanocomposites. *Journal of Alloys and Compounds*, Vol. 696, 2017, pp. 1342–1348.

[224] Liu, Y., J. L. Lan, B. P. Zhang, Y. H. Lin, and C. W. Nan. Thermoelectric transport properties of BiCuSeO with embedded La0.8Sr0.2CoO3 nanoinclusions. *Science China. Technological Sciences*, Vol. 59, No. 7, 2016, pp. 1036–1041.

[225] Yang, S. D., J. Si, Q. Su, and H. Wu. Enhanced thermoelectric performance of SnSe doped with layered MoS2 /graphene. *Materials Letters*, Vol. 193, 2017, pp. 146–149.

[226] Feng, D., Y.-X. Chen, L.-W. Fu, J. Li, and J.-Q. He. SnSe+ Ag2Se composite engineering with ball milling for enhanced thermoelectric performance. *Rare Metals*, Vol. 37, No. 4, 2018, pp. 333–342.